ORNL-3230
UC-25 – Metals, Ceramics, and Materials
TID-4500 (16th ed., Rev.)

EFFECT OF HEAT FLUX ON THE CORROSION OF ALUMINUM BY WATER

PART III. FINAL REPORT ON TESTS RELATIVE TO THE HIGH-FLUX ISOTOPE REACTOR

J. C. Griess
H. C. Savage
J. G. Rainwater
T. H. Mauney
J. L. English

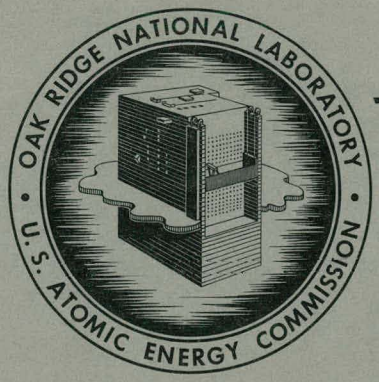

OAK RIDGE NATIONAL LABORATORY
operated by
UNION CARBIDE CORPORATION
for the
U.S. ATOMIC ENERGY COMMISSION

DISCLAIMER

Printed in USA. Price $1.25 . Available from the

Office of Technical Services
Department of Commerce
Washington 25, D.C.

ORNL-3230

Contract No. W-7405-eng-26

REACTOR CHEMISTRY DIVISION

EFFECT OF HEAT FLUX ON THE CORROSION OF ALUMINUM BY WATER

PART III. FINAL REPORT ON TESTS RELATIVE TO THE HIGH-FLUX ISOTOPE REACTOR

J. C. Griess, H. C. Savage, J. G. Rainwater, T. H. Mauney, and J. L. English

DATE ISSUED

DEC 20 1961

OAK RIDGE NATIONAL LABORATORY
Oak Ridge, Tennessee
operated by
UNION CARBIDE CORPORATION
for the
U. S. ATOMIC ENERGY COMMISSION

THIS PAGE

WAS INTENTIONALLY

LEFT BLANK

CONTENTS

EFFECT OF HEAT FLUX ON THE CORROSION OF ALUMINUM BY WATER PART III. FINAL REPORT ON TESTS RELATIVE TO THE HIGH-FLUX ISOTOPE REACTOR

J. C. Griess, H. C. Savage, J. G. Rainwater,* T. H. Mauney, and J. L. English

ABSTRACT

The effect of very high heat fluxes on the corrosion of 1100 and 6061 aluminum alloys by water was investigated. The purpose of the investigation was to determine whether aluminum would have adequate corrosion resistance for use as a fuel-element cladding material in the High-Flux Isotope Reactor; therefore the test conditions generally simulated those expected to exist during reactor operation.

At heat fluxes between 1 and 2 x 10^6 Btu/hr·ft^2 and with coolant temperatures and velocities in the ranges of 131 to 250°F and 31 to 51 fps, respectively, a layer of boehmite ($\alpha Al_2O_3 \cdot H_2O$) which has low thermal conductivity, formed on the water-cooled aluminum surfaces during test. When only relatively thin films formed, the boehmite adhered tightly to the aluminum, but in those cases where relatively thick films formed, some boehmite spontaneously spalled from the surface. The rate at which the boehmite formed on the surface (and consequently the rate at which the aluminum temperature increased) was a function of the temperature at the specimen-water interface and the pH of the coolant. The lower the temperature and the lower the pH (in the range of 5.0 to 6.5 with HNO_3), the lower the rate of corrosion-product formation. Within the ranges investigated, pressure and flow rate were without effect, and the same results were obtained with 6061 and 1100 aluminum.

In those cases where the pH of the coolant was adjusted to 5, corrosion penetration was uniform and even under the most severe conditions did not exceed 1.5 mils in 10 days. When the test conditions were such that the rate of oxide formation was high and oxide spalled from the surface of the specimen, localized attack of the aluminum in the form of subsurface voids extending several mils into the metal was always observed.

From the experimental data, fluid-film heat-transfer coefficients were calculated and the thermal conductivity of the corrosion product was estimated. The fluid-film heat-transfer coefficients were in excellent agreement with those determined by others under similar conditions, and a value of 1.3 ± 0.2 Btu/hr·ft^2·°F/ft was obtained as the thermal conductivity of the corrosion-product film.

The results obtained in this test program indicate that from a corrosion standpoint either 6061 or 1100 aluminum could be used as cladding material for the High-Flux Isotope Reactor fuel elements, provided the pH of the coolant is maintained at 5.0 to 5.3 with nitric acid. Under test conditions simulating the most severe conditions anticipated during operation of the reactor (hot spot - hot channel) the maximum penetration observed was only 1 mil in 10 days. Although somewhat excessive temperatures are probable at hot spots due to a high rate of corrosion-product buildup, the great majority of the fuel plates will operate at reasonable temperatures.

*Summer research participant from the University of Arkansas.

INTRODUCTION

A study of the effect of high heat fluxes on the corrosion of aluminum by water was undertaken at this laboratory to determine whether aluminum-clad fuel elements could be satisfactorily used in the High-Flux Isotope Reactor (HFIR). The design features of this reactor have been described elsewhere,[1,2] but it should be noted that 0.050-in.-thick fuel plates which contain a nominal 30-mil fuel region and 10 mils of sheathing on each side will be used and that heat fluxes as high as 1.52×10^6 Btu/hr·ft^2 (hot spot - hot channel condition) will exist during reactor operation. The nominal cooling-water temperature will be 120 to 190°F, but when hot-channel factors are considered, water temperatures as high as 236°F are possible and fuel-element surface temperatures as high as 344°F could exist.[3] Because of the high power density at which the reactor will operate, each fuel loading will only last about two weeks. Consequently corrosion rates of the cladding material considerably in excess of those that could be tolerated in a normal pressurized-water power reactor or in a water-cooled research reactor are practicable in the HFIR.

As shown in previous reports,[4,5] the corrosion of aluminum in water leads to the formation of an adherent layer of corrosion products which is a barrier to heat transfer. (In the tests conducted in this program the only corrosion product identified was boehmite, $\alpha Al_2O_3 \cdot H_2O$.) Thus as an aluminum specimen corrodes at constant heat flux, the temperature of the specimen increases as corrosion proceeds. Since both the normal aluminum cladding alloys and the fuel (either uranium-aluminum alloy or a dispersion of U_3O_8 in aluminum) have low strength, any determination of the adequacy of aluminum-clad fuel plates must consider not only corrosion damage as such but also the temperatures which will be produced in the fuel plates during reactor operation. If fuel-element temperatures become too high, buckling and/or creep may limit the use of the fuel plates more so than corrosion damage, per se. Thus in this investigation it was important to determine corrosion damage to aluminum cladding materials, the rate of corrosion-product formation on the heat-transfer surface, the thermal conductivity

of the corrosion products, and fluid-film heat-transfer coefficients under conditions approximating those expected to exist during operation of the HFIR.

This report contains data that have been collected since the last report in this series was written[5] and evaluates all of the data that have been obtained in this part of the HFIR development program.

EXPERIMENTAL PROCEDURES

The experimental equipment and the technique used in this investigation have been described in detail in a previous report,[4] and only a brief description of the equipment and procedures is presented here. A 6.5-in.-long aluminum specimen with a center rectangular flow channel 0.050 by 0.500 in. in cross section was heated by passing 60-cycle a-c current through it. Large aluminum electrodes, to which the power leads from the transformer were attached and by means of which the specimen was flanged into a loop, were welded to the ends of the specimen. Heat was removed by water flowing through the channel. The temperature of the specimen was monitored by means of thermocouples spot-welded on the outside surface of the specimen. Micalex insulators surrounded the specimen to minimize loss of heat to the air, and the insulators were backed up with stainless steel plates so that the specimen could withstand internal pressures up to at least 1000 psi. Figure 1 is a sketch of the specimen showing the location of the thermocouples and the cross-sectional dimensions of the specimen. In the experiments described in this report the location and designation of the thermocouples were the same in all runs. The geometry of the specimen was such that 80% of the power was generated in the 0.100-in.-thick portions and the remainder in the 0.025-in.-thick sections. Considering relative areas available for heat transfer, the heat flux at the cooled surface under the thicker section was 3.3 times greater than that under the thin sections.

The test specimens used in the first several experiments were made by drilling an aluminum rod to the proper diameter, flattening it on a mandrel to form the flow channel, and then machining the outside edges to the cross section shown

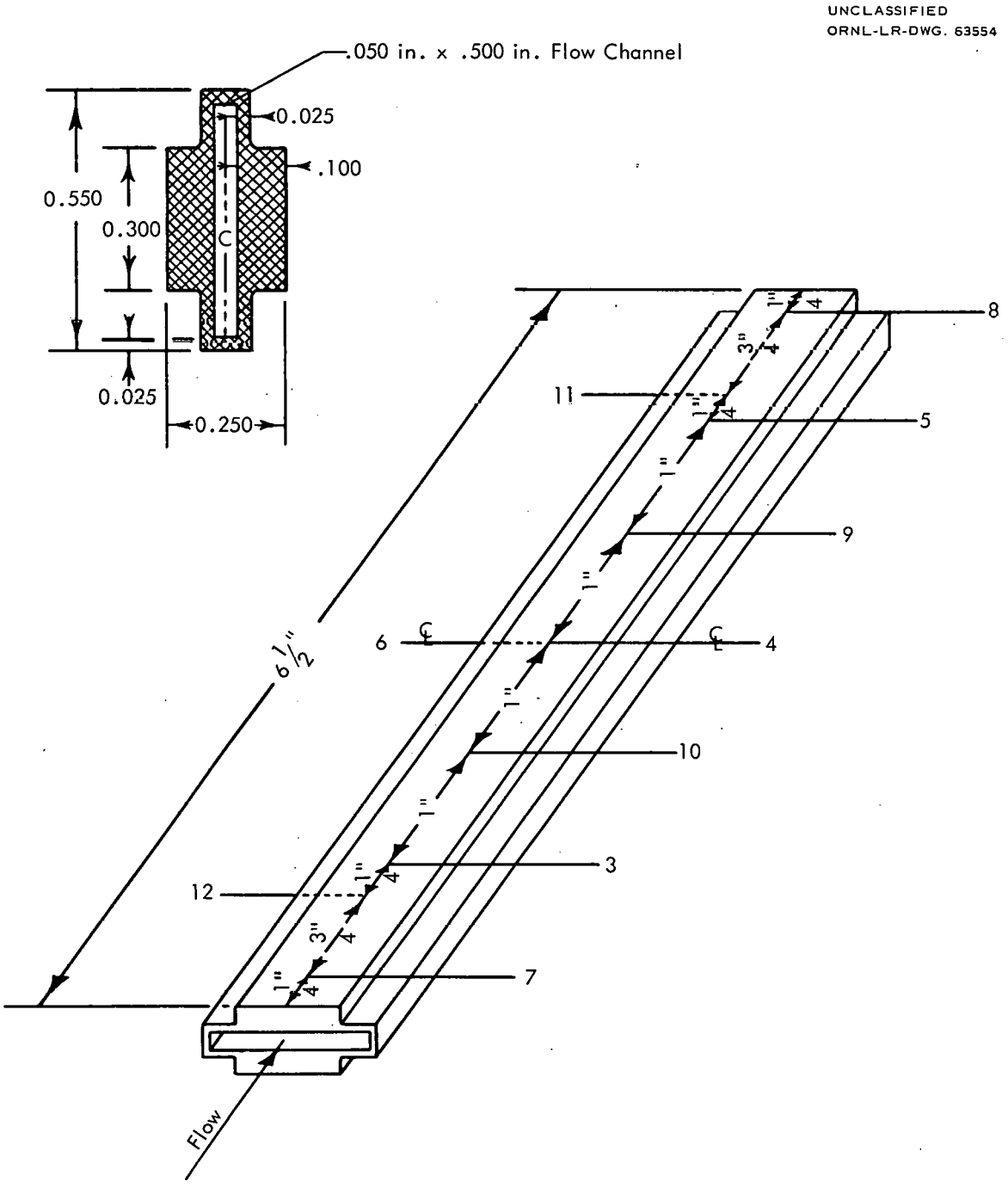

Fig. 1. Sketch of Specimen Showing Dimension and Thermocouple Locations.

in Fig. 1. The test specimens used in the latter part of this investigation were made by machining two axial halves of each specimen from plate and then joining them by welding on the sides. With the former specimens it was impossible to determine corrosion penetrations quantitatively; with the latter type specimen, the loss in thickness during a run could be determined.

Prior to welding, the specimen was thoroughly cleaned with acetone and alcohol. After joining the two halves of the specimen and welding it to the electrodes, the interior surface of the specimen was cleaned by exposure to three portions of a 50% (volume) solution of nitric acid at 120 to 140°F for a total of 30 minutes. After thorough rinsing with deionized water, the specimen was ready for test.

The test specimen was installed in a bypass line of a stainless steel pump loop. The flow of cooling water through the test specimen was controlled by a throttling valve, and an indicator-recorder continuously monitored the flow rate. All of the experiments were conducted in the same loop.

The entire test system contained 25 liters of coolant, the quality of which was maintained by passing about a 3.5 liters/hr side-stream through an ion-exchange bed. In those cases where high-purity water was the coolant, a mixed-bed ion column was used, and the specific resistance of the water in the loop usually was about 1×10^6 ohm-cm. When it was desired to maintain a low concentration of acid in the water, the proper amount of nitric acid was added to the system and a cation exchanger in the hydrogen form was used instead of the mixed-bed exchanger. In the latter case the pH of the coolant was usually maintained within ± 0.1 pH unit of the desired value.

The system pressure was regulated by means of a letdown valve and feed pump.

The original estimate of the lifetime of an HFIR core was 10 days, and for this reason most of the tests were of that duration. Except for one case, experiment A-10, which was previously described[5] and will not be discussed in this report, the conditions during a run were kept as constant as possible.

The test designations and operating conditions are shown in Table 1. Tests A-1 and A-15 were carried out to check performance of the equipment, and no

Table 1. Test Conditions

Test No.	Average Heat Flux* (Btu/hr·ft^2 x 10^{-6})	Coolant Temperature (°F)		Coolant Flow Rate (fps)	Center Temperature of Specimen (°F)		Pressure (psig)	Alloy	Run Time (hr)	Water Condition (pH)
		Inlet	Outlet		Initial	Final				
A-2	1.70	152	189	41	341	456	300	1100	240	Deionized
A-3	1.63	151	190	37	316	442	900	1100	129	Deionized
A-6	1.70	153	193	38	316	455	900	1100	240	Deionized
A-7	1.58	157	194	38	314	349	900	1100	240	5.0
A-8	1.58	154	191	37	306	343	900	1100	240	5.0
A-9	1.57	186	227	35	344	394	900	1100	240	5.0
A-11	1.57	153	195	33	349	362	900	6061-T6	240	5.0
A-12	1.51	166	193	51	304	320	900	6061-0	240	5.0
A-13	1.64	131	173	35	312	320	900	6061-0	240	5.0
A-14	1.35	190	220	40	337	379	900	6061-0	240	5.0
A-16	1.55	185	219	41	325	399	60	6061-0	480	5.0
A-17	2.05	174	218	41	434	440	70	6061-0	240	5.0
A-18	2.06	174	219	41	391	498	900	6061-0	240	5.0
A-19	1.93	179	218	41	377	424	80	6061-0	241	5.0
A-20	2.00	181	218	42	383	504	920	6061-0	240	5.3
A-21	2.03	176	220	41	374	578	900	6061-0	240	5.7
A-22	0.94	198	219	41	316	335	910	6061-0	240	5.0
A-23	2.05	175	218	41	386	676	900	6061-T6	240	Deionized
A-24	1.65	210	250	37	386	485	950	6061-0	240	5.0

*Average heat flux for the whole specimen for the duration of the test.

corrosion data were obtained from these tests. Tests A-4 and A-5 are not shown in the table because they were abnormal and have already been discussed.[5] The average heat fluxes shown for tests through A-13 are slightly different from those listed previously.[5] These changes resulted from re-evaluation of the experimental data as described in a later section. The initial and final specimen temperatures presented in columns 5 and 6 are the average temperatures determined by thermocouples 4 and 6 (Fig. 1) which were located on the outside of the specimen at the midpoint. These midpoint temperatures represent approximately the range of average specimen temperatures during the test.

At the conclusion of a test the specimen was removed from the loop and the edges were machined off so that the interior surfaces could be examined. Parts of the specimen were sectioned, mounted in Bakelite, metallographically polished, and examined microscopically to determine the thickness of the corrosion-product layer and the extent and type of localized attack. When the welded type of specimen was used, all of the specimen except that used for metallographic examination was electrolytically descaled as described by Draley,[6] and the extent of uniform corrosion was determined. The depth of penetration was obtained by carefully measuring the thickness of each half of the specimen at several points in the transverse center of the specimen before assembly and then measuring the thickness at the same locations after removal of the corrosion products. The accuracy of each thickness measurement was estimated to be $\pm$0.0001 in.

EXPERIMENTAL RESULTS

Specimen Temperatures

Ten thermocouples were attached to the outside of each specimen, and these were used to monitor the temperature of the specimen during each test. At the start of a test when the specimen had no significant oxide coating on it, the temperatures measured on the outside of the specimen agreed reasonably well with calculated values. During each test the temperature increased at all locations on the specimen as a layer of corrosion products formed on the water-cooled

surfaces. In most cases the temperature increased nearly linearly throughout the test period, indicating that the corrosion product was forming at approximately a constant rate. An example of this behavior is shown in Fig. 2 where the temperatures measured by three thermocouples during test A-14 are plotted vs. time. The small, irregular fluctuations in the temperature curves were due to slight, irregular fluctuations in power input and coolant temperature.

In one case, test A-17, the behavior was abnormal in that the temperature increased rapidly at the start of the test, then decreased, and slowly increased again. Figure 3 shows the temperature vs. time plot at three thermocouple locations. This behavior was shown only by this one test, and no explanation for it can be given at this time. However, it should be noted (see Table 1) that the initial temperature at the center of the specimen was unaccountably substantially higher than that for tests A-18 and A-23 which had very nearly the same heat flux, flow rate, and coolant temperature.

In a few cases where relatively thick corrosion-product films formed, the temperature increased linearly for several days and then decreased as some corrosion product was lost from the water-cooled surface. Such temperature behavior is illustrated in Fig. 4 for thermocouple 11 during test A-21. Note that in this run the rate of temperature increase (and total corrosion-product thickness) was much greater than that in test A-14 as shown in Fig. 2.

Table 2 shows the rates of temperature increase observed at all thermocouple locations in all runs except A-17. In those cases where, after several days of test, the temperature leveled off and then decreased, the rate of temperature increase during the first part of the run, which was linear, is shown in the table. The rate shown is the slope of the best straight line drawn through the temperature vs. time plot. The data for the runs through A-13 were previously presented[4,5] but are included here for completeness.

It should be noted that the rates of temperature increase shown in Table 2 are not highly precise and are intended to show relative effects of certain variables. The temperatures and the rates of temperature increase at thermocouple

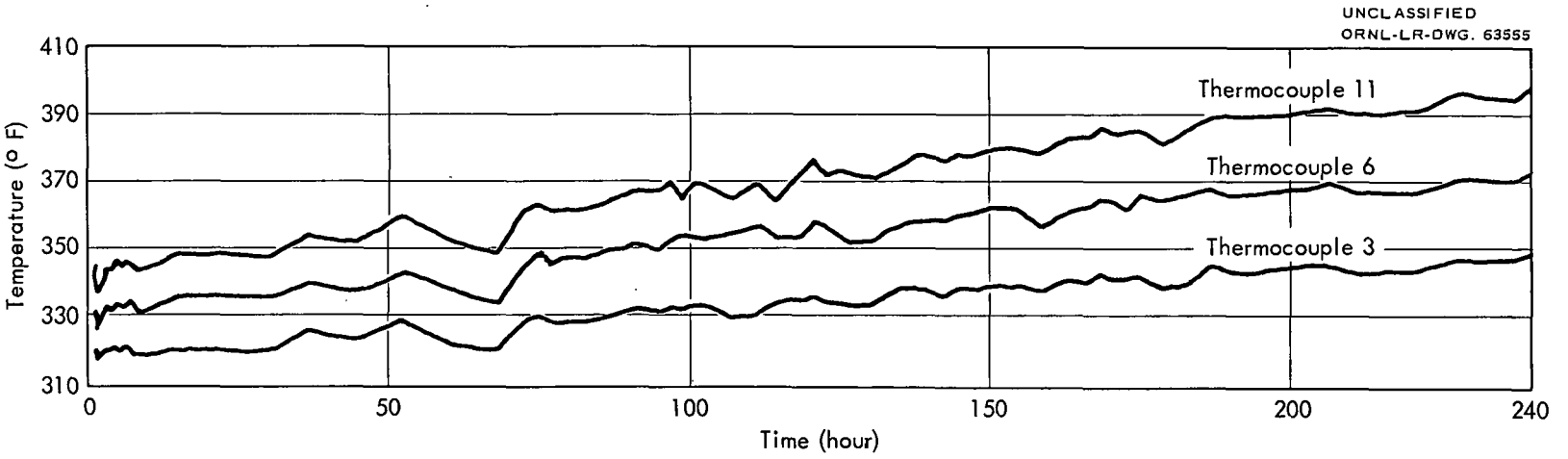

Fig. 2. The Temperature at Three Thermocouple Locations During Test A-14.

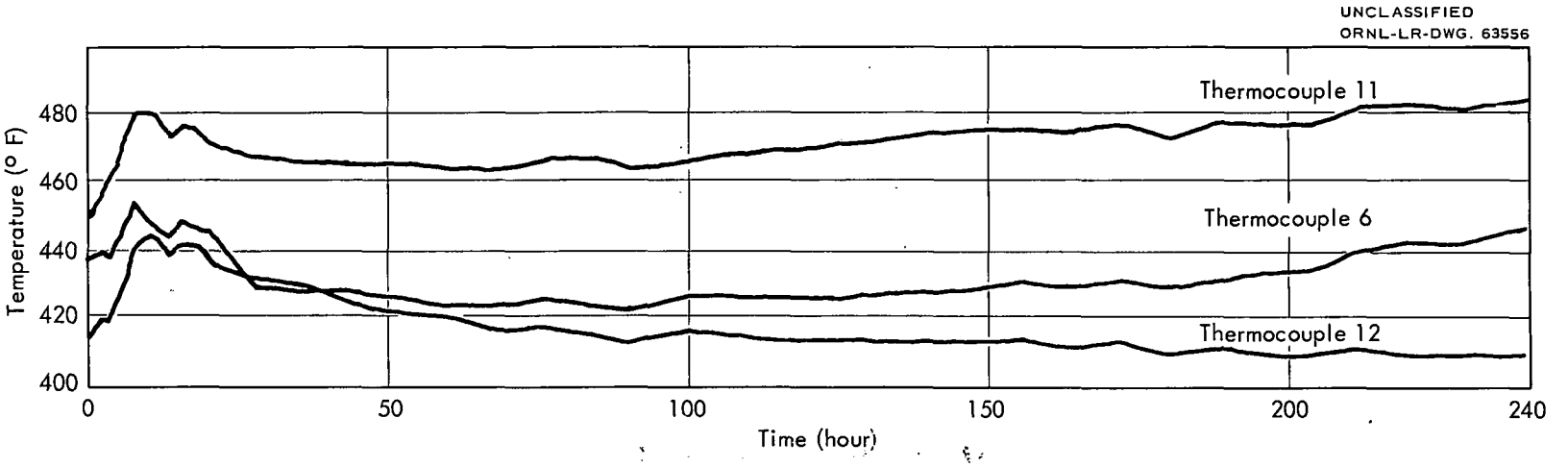

Fig. 3. The Temperature at Three Thermocouple Locations During Test A-17.

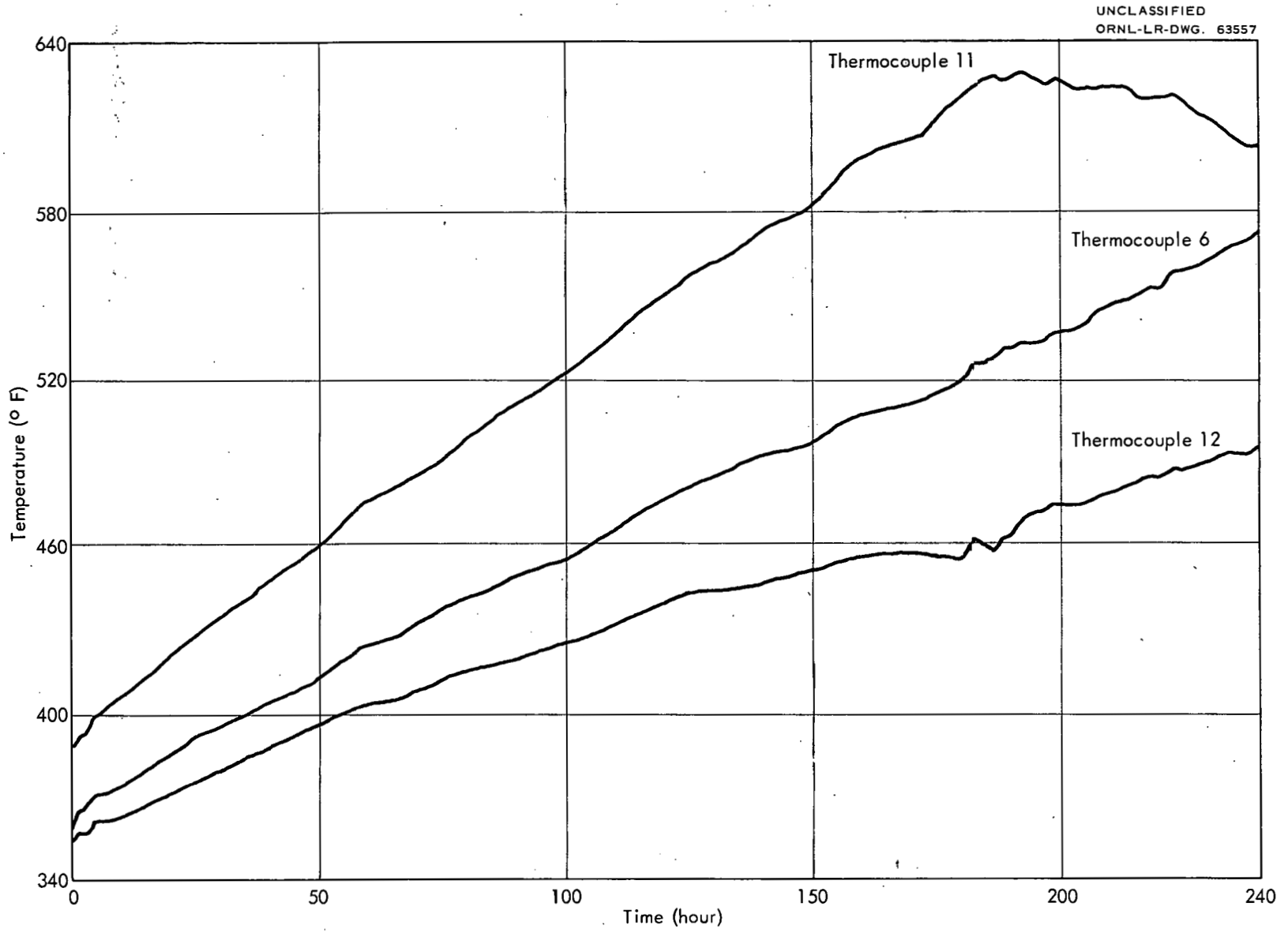

Fig. 4. The Temperature at Three Thermocouple Locations Durirg Test A-21.

Table 2. Rate of Temperature Increase of Aluminum Specimens During Tests

Test Designation	Rate of Temperature Increase (°F/day) Thermocouple Designation[a]									
	7[b] (1/4)	12 (1)	3 (1 1/4)	10 (2 1/4)	4 (3 1/4)	6 (3 1/4)	9 (4 1/4)	5 (5 1/4)	11 (5 1/2)	8[b] (6 1/4)
A-2[c]	-	4.9	4.5	5.9	8.6	9.9	11.2	-	18.0[d]	12.4
A-3	8.3	14.8	-	17.3	24.0	24.0	26.0	29.0	34.0	24.0
A-6	3.4	9.4	9.9	13.0	13.5	14.8	16.8	19.0	22.0	16.2
A-7	1.3	2.2	2.0	2.5	3.4	3.4	3.6	5.2	6.1	5.0
A-8	0.4	1.3	1.8	2.2	1.8	-	2.9	4.1	3.6	2.2
A-9	1.8	3.2	3.1	4.0	4.1	4.3	5.0	5.9	5.9	5.6
A-11	0.4	1.3	1.4	1.8	-	1.8	2.0	3.4	3.8	3.1
A-12	0.9	1.3	1.4	2.0	1.8	1.8	2.2	2.9	2.7	1.8
A-13	<0.2	0.2	0.2	0.3	0.4	0.2	0.4	0.7	0.4	0.4
A-14	2.3	-	3.0	3.4	4.0	4.3	-	4.3	5.6	4.3
A-16[c]	1.6	2.5	2.0	2.4	3.0	3.7	3.3	3.7	4.3	2.8
A-18	4.1	4.9	7.2	7.2	11.0	9.9	12.8	14.9	16.9	12.4
A-19	1.8	3.1	-	3.8	4.9	3.2	6.5	6.8	8.5	6.3
A-20	2.7	8.1	8.8	-	12.8	12.2	14.2[d]	14.6[d]	17.3[d]	12.4[d]
A-21	6.7	14.0	15.5	18.9	20.7	21.1	24.5[d]	29.5[d]	31.3[d]	18.9[d]
A-22	-	0.7	1.8	1.8[d]	1.8[d]	-[d]	2.2[d]	2.2[d]	2.2[d]	1.1[d]
A-23	9.2	22.7	22.5	28.4[d]	36.7[d]	38.5[d]	40.0[d]	43.9[d]	45.0[d]	31.7[d]
A-24	4.1	6.1	6.5	7.6	8.8	8.5	9.4	12.5	13.0	9.5

[a] The numbers in parentheses indicate the distance (inches) of the thermocouple from the entrance end of the specimen.
[b] Rate of temperature increase probably low because of proximity to large electrodes.
[c] Tests A-1 and A-15 were runs made to check the loop system and data were not obtained from these tests.
[d] Rate based on initial test period, following which the corrosion products began sloughing off the specimen.

locations 7 and 8 were lower than expected in nearly all tests. Each of these thermocouples was located 1/4 in. from either the inlet or outlet of the specimen, the ends of which were welded to large aluminum electrodes. The electrodes were considerably cooler than the specimen and served as heat sinks, a fact that caused lower temperatures at the end locations. Therefore the data obtained from thermocouples 7 and 8 were not used in the final analysis of the data. It has already been shown that test A-17 was unusual, and additional data to be presented further substantiate this claim. Consequently all of the data from this run were disregarded in correlating the results.

Effect of pH. The most significant variable in controlling the rate of oxide formation was the concentration of nitric acid in the water. When the coolant was made slightly acid, the rate of temperature increase (oxide formation) was less than when the coolant was deionized water. A comparison of tests A-2, A-3, and A-6 with tests A-7 and A-8 makes this point evident. All five tests were made under nearly the same conditions except in the former group the coolant was deionized water, whereas in the latter two runs the water was adjusted to a pH of 5. From Table 2 it can be seen that the rates of temperature increase in tests A-7 and A-8 were much lower than in runs A-2, A-3, and A-6. A similar comparison can be made between tests A-18 and A-23 where the operating conditions were the same except in the former test the coolant was water at a pH of 5, whereas deionized water was used in the latter case. Again the rates of temperature increase were much lower in test A-18 than in A-23.

Runs A-18, A-20, A-21, and A-23 were made under nearly identical conditions except the pH of the coolant was different in each run. Figure 5 shows how the rate of temperature increase changed as a function of pH at three locations on the specimens. (The data for all thermocouple locations are shown in Table 2.) The measured pH of the deionized water was about 6.5, and this value was used in the graph. It can be seen from the graph that at all three locations on the specimen the rate of temperature increase was greater the higher the pH, although the difference between pH 5.0 and pH 5.3 was very small at thermocouple 11.

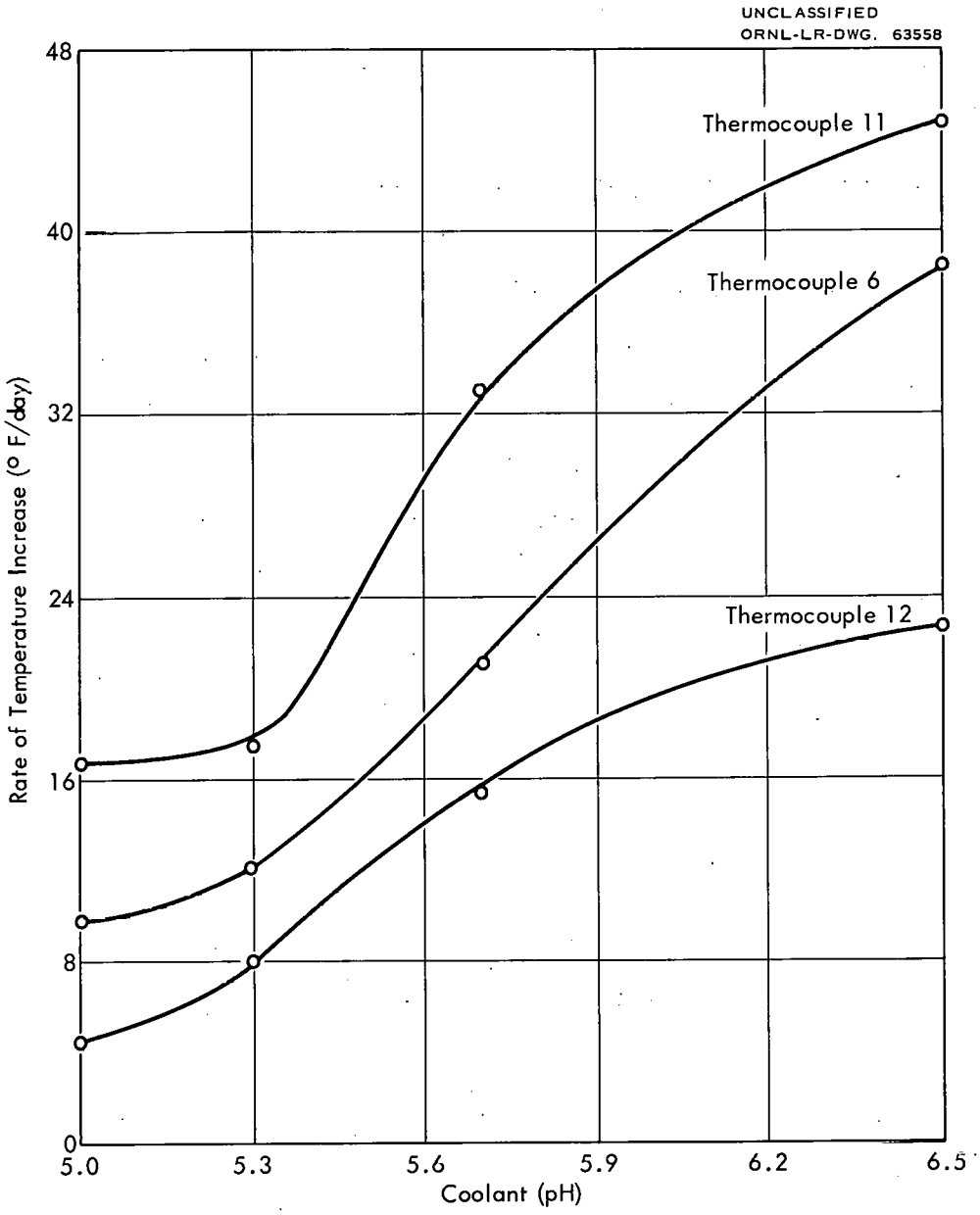

Fig. 5. The Effect of pH on the Rate of Temperature Increase in Aluminum Corrosion Specimens Subjected to a Heat Flux of 2×10^6 Btu/hr·ft^2 and Cooled by Water.

A minimum in the rate of temperature rise vs. pH curve must exist, since in one brief period during test A-10 where the pH of the water was adjusted to 4 with nitric acid and the heat flux was 1.5×10^6 Btu/hr·ft^2 an extremely high rate of temperature increase (200 to 300°F/day) was observed.[5] In this program pH values between 4 and 5 were not explored.

The Effect of Alloy Composition. The first tests were conducted with specimens fabricated from 1100 aluminum, and the later tests used 6061 aluminum specimens. Comparison of the rates of temperature increase in test A-9 where an 1100 aluminum specimen was employed with those in test A-14 where the conditions were about the same except a 6061 aluminum specimen was used shows that there was no major difference between the results in the two tests. A similar conclusion can be reached by comparing test A-8 (1100) with test A-11 (6061). The above observations and the fact that the composition and thermal conductivity of the corrosion product were the same regardless of alloy (see later section) have led to the conclusion that in the temperature range investigated there was no significant difference in the rate of oxide formation (and presumably corrosion) on the two alloys under the same conditions of test. In isothermal tests of 10-day duration[7] the two alloys showed similar corrosion rates and thus the similarity in the heat throughput tests was expected.

The Effect of Heat Flux, Coolant Temperature, and Flow Rate. From Tables 1 and 2 it can be concluded that other conditions remaining the same, the higher the heat flux or the higher the temperature of the coolant, the greater the rate of temperature increase. Within the rather narrow range investigated flow rate did not appear to be a major variable. These facts suggested the possibility that the rate of corrosion-product buildup on the specimen (and thereby the rate of temperature increase) was not directly dependent on the heat flux but that heat flux was important in that it influenced the specimen temperatures. Therefore an attempt was made to correlate the rate of oxide formation with specimen temperatures.

It was observed that in nearly all cases the rate of oxide accumulation was constant throughout the run although the temperature of the metal and the average temperature of the oxide increased substantially during most runs. The temperature at the specimen-water interface,* however, was essentially constant during any run, and it was this latter temperature that was used in the correlation. Since the rate of oxide buildup on the specimen was probably related to the rate of corrosion and since the corrosion rate of aluminum as a function of temperature follows an Arrhenius-type relationship,[8,9] the rate of oxide accumulation on the surface was also plotted in this manner. Figure 6 is a plot of the logarithm of the rate of oxide accumulation on the specimen surface versus the reciprocal of the absolute temperature at the specimen-water interface. All of the data obtained in water at a pH of 5 are included on the plot regardless of alloy, heat flux, flow rate, pressure, or coolant temperature. To normalize the data obtained at the different heat fluxes to a common basis it was necessary to use the rate of oxide formation on the surface rather than the rate of temperature rise. The rate of oxide accumulation was determined by measuring the oxide thickness at several locations on each specimen at the end of the test as described in a later section (see Table 4), and assuming that it formed at a constant rate during the exposure. Each specimen-water interface temperature was determined from the thermocouple at that location or from one no more than 1/4 in. away, assuming no oxide on the specimen at the start of the test and allowing for the temperature drop through the aluminum.

Although the data scatter considerably around the least-squares line drawn through the points, the agreement is considered satisfactory in view of the nature of the experiments. Thus Fig. 6 implies that in those tests conducted at a pH of 5 the rate of oxide formation was a function of the temperature at the specimen-water interface and that heat flux, flow rate, and coolant temperature in the ranges investigated were important only in that they affected this temperature.

*At the start of a test the specimen-water interface was the aluminum-water interface; after oxide formed on the surface, it was the aluminum oxide-water interface.

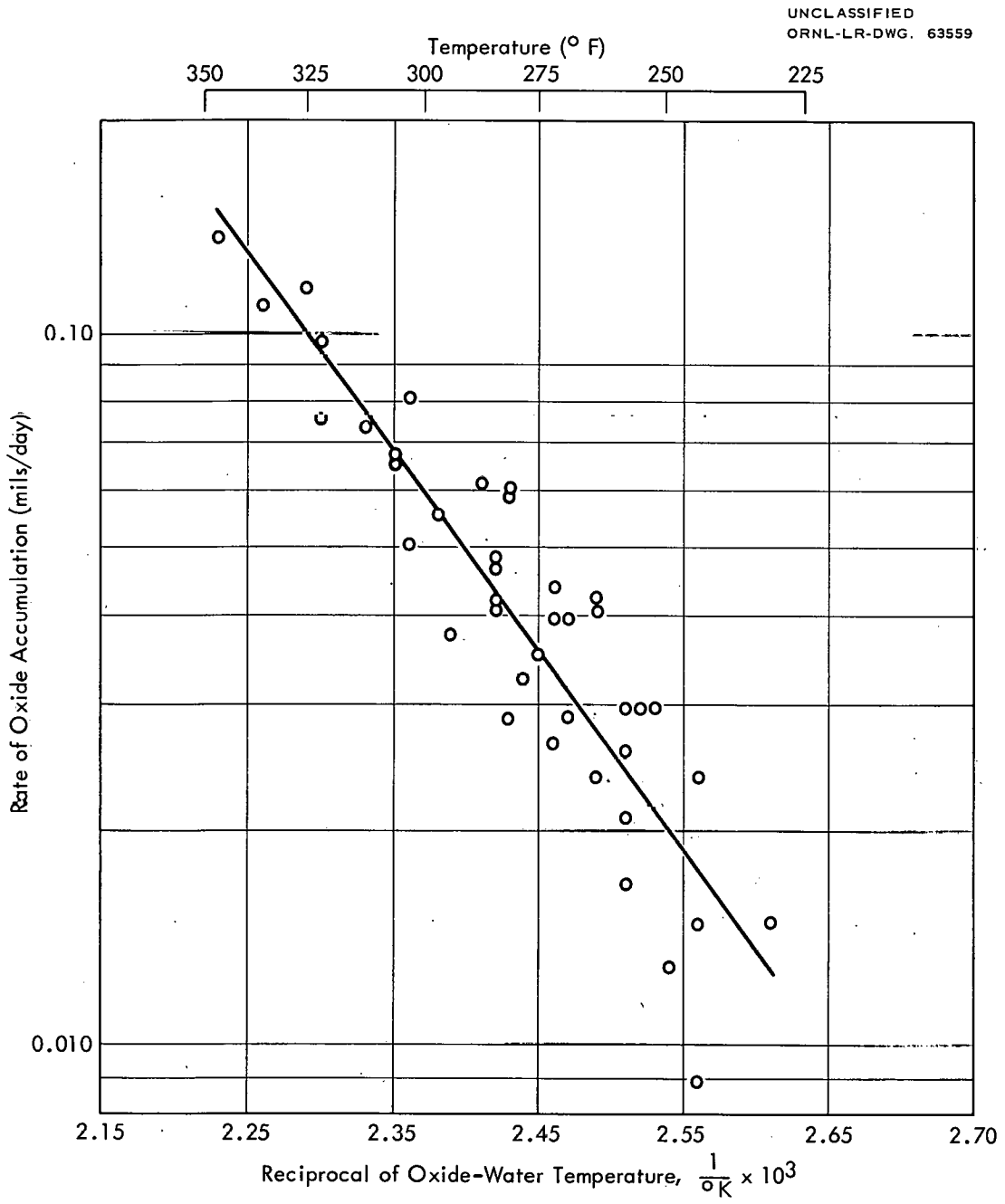

Fig. 6. The Rate of Corrosion-Product Formation on Aluminum Corrosion Specimens Subjected to Heat Fluxes of 1 to 2 x 10^6 Btu/hr·ft^2 and Cooled by Water Adjusted to pH 5 with HNO_3

Too few runs were conducted at pH values greater than 5 to determine whether a similar type of correlation existed. Certainly if it did exist, the location of the curve would lie above that drawn for the data obtained at a pH of 5.

Effect of Time. As is evident from Table 2, only one run, A-16, lasted longer than 10 days, and no detailed statements can be made concerning the effect of time. However, tests A-14, which lasted 10 days, and A-16, which lasted 20 days, were run under similar conditions except for pressure and a slight difference in heat flux, and in each test the rate of oxide formation was constant for the duration of the test. The rate of formation of oxide appeared to be slightly lower in test A-16 than in A-14, a fact probably related to the lower surface temperature in test A-16.

Certainly the rate of temperature increase would not remain linear indefinitely, and at some oxide thickness probably dependent on the conditions, the rate of oxide formation on the aluminum would decrease and some oxide might even be lost from the aluminum surface. Such was the case on parts of the specimens in tests A-2, A-21, and A-23.

Effect of Pressure. All of the tests were conducted at pressures such that boiling could not occur at the specimen-water interface during a test. However, in tests A-16, A-17, and A-19 the system pressure was low enough so that at some stage during the test boiling could have occurred at the metal - metal oxide interface or even in the corrosion product itself had water been present. It might therefore be expected that differences in results would exist between the high- and low-pressure runs. Although the data presented in Table 2 indicate that lower rates of temperature increase were noted in the low-pressure runs than in similar high-pressure runs, it should be noted from Table 1 that the specimen temperature was usually also lower. Furthermore, the data plotted in Fig. 6 are for all runs in which the pH of the coolant was 5, regardless of pressure, and there appeared to be no significant difference in the fit of the points to the line at all pressures. It is therefore tentatively concluded that at pressures

sufficiently high to prevent surface boiling, pressure is not an important variable in determining the rate of corrosion-product formation.

Specimen Examination

At the conclusion of each test the specimen was cut from the aluminum electrodes and the sides of the specimen were milled off to separate the two halves of the specimen and to expose the water-cooled surfaces. These surfaces were examined microscopically and several metallographic sections were made to determine the type and extent of attack and the thickness of the oxide. When the welded-type specimens were used, the oxide was removed from the surface and the loss in thickness of the specimen during the test was determined.

Surface Examination. In those cases where the temperature of the specimen continued to increase during a run, the specimen surface at the end of the test looked much as it did before the test except in a few cases there was a slight reddish-brown surface discoloration due to traces of iron and chromium oxides originating from the stainless steel loop. However, careful microscopic examination revealed that in all cases a thin, nearly transparent layer of corrosion products was present on the metal surfaces. This oxide film appeared to be tightly adherent and free of defects, but when heated slightly by the microscope lamp during viewing, cracks could be observed forming on the surface; there was, however, no tendency for the oxide to spall. Figure 7 is a macroscopic view of such a specimen.

In those locations on a specimen where the temperature went through a maximum and then decreased, some oxide was lost from the specimen. This phenomenon has been referred to as "film stripping." Figure 8 is a photograph of specimen A-23 on which the stripping extended almost the entire length of the specimen. An enlargement of the stripped area is shown in Fig. 9 where the irregular oxide deposit can be seen. In certain areas white oxide deposits were as thick as several mils, and in other areas the metal appeared to have practically no oxide on it. The irregular nature of the oxide deposit in the stripped areas probably

T19921

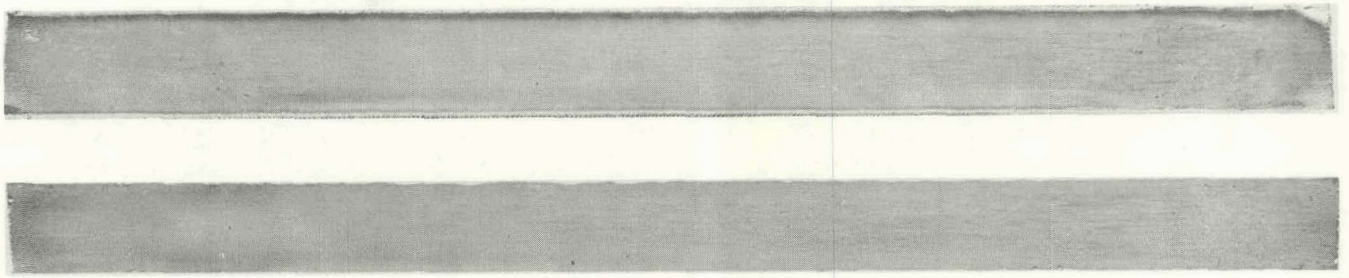

Fig. 7. The Appearance of the Specimen at the End of Test A-18.
Flow Was from Left to Right.

T20058

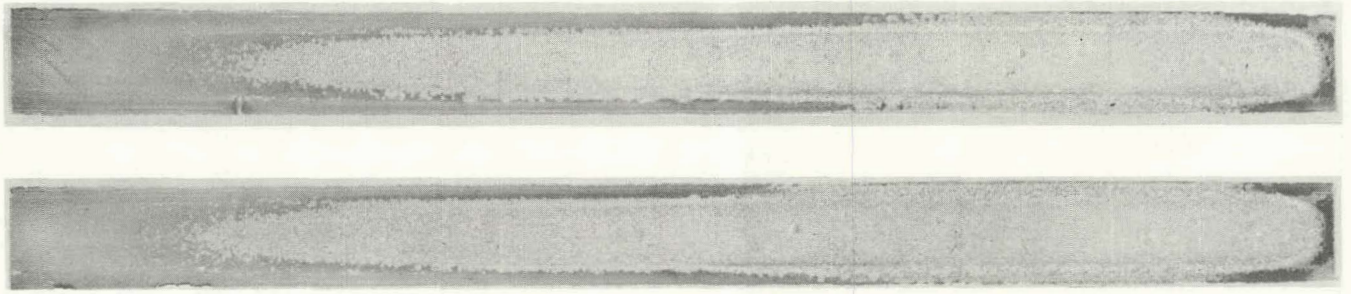

Fig. 8. The Appearance of the Specimen at the End of Test A-23.
Flow Was from Left to Right.

T20061

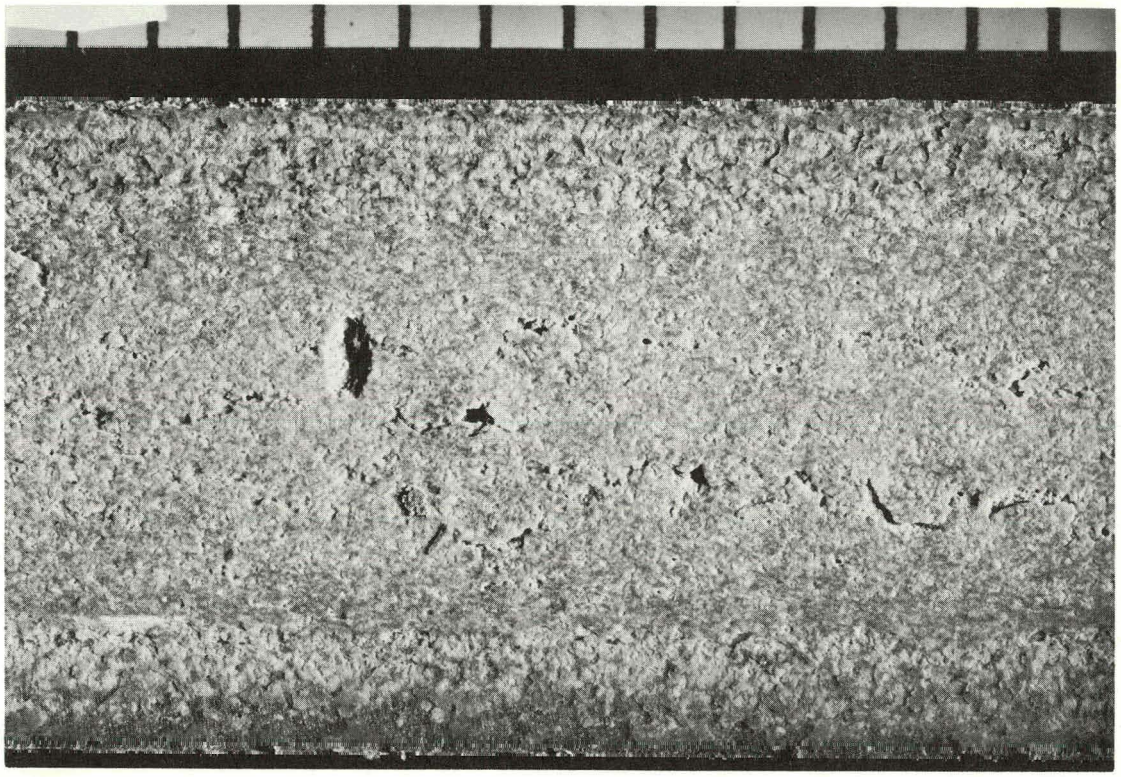

Fig. 9. An Enlarged View of the Surface of Specimen A-23 Taken 2 in. from the Specimen Outlet. Note Irregular Oxide Deposit. (Magnification 7.8X)

accounted for the large temperature fluctuations sometimes observed in those tests where stripping occurred.

Composition of Corrosion Product. Although no detailed study was made, the corrosion product formed on several of the specimens was examined by x-ray diffraction, electron diffraction, chemical analyses, and/or emission spectrography. Small amounts of corrosion products scraped from specimens A-2, A-7, and A-23 and subjected to x-ray examination yielded identical diffraction patterns which indicated only the presence of boehmite, $\alpha Al_2O_3 \cdot H_2O$. A sample of the oxide removed from specimen A-7 was also examined spectrographically; except for traces of iron, calcium, and magnesium, the spectrogram indicated only aluminum.

A reflection electron diffraction technique was used to determine whether the oxide that was nearly transparent and adhered well to the aluminum was the same as the irregular white material found in the film-stripped regions on a few

specimens. Using one side of the specimen from test A-21 with the corrosion-product film in place, reflection electron diffraction patterns were obtained from a region about 1 in. from the inlet end (unstripped area) and 1 in. from the outlet (stripped area). The patterns obtained were identical and corresponded to boehmite.

Chemical analyses were performed on samples of corrosion product carefully scraped from the surface of specimens A-6 and A-23. The results of these analyses and those previously reported for the corrosion product formed on specimen A-10[5] are shown in Table 3.

Table 3. The Chemical Composition of Oxide Films

Test Number	Composition (wt %)			
	Al	Fe	Ni	Cr
A-6	36.5	0.9	<0.2	0.6
A-10	39.8	1.1	0.2	0.1
A-23	40.8	0.5	<0.1	0.2

Since pure $Al_2O_3 \cdot H_2O$ contains 45% aluminum, the results of the chemical analyses suggest that some other substance, probably water, was present in the corrosion product. In view of the fact that samples were dried at only 80°C before weighing for analyses, the less than stoichiometric quantity of aluminum was not unexpected. Furthermore, only very small samples of corrosion product were available for chemical analyses, a fact which would tend to reduce the accuracy.

Although only a limited number of examinations were made, it can be concluded that at least the major portion of the corrosion product formed on the aluminum surfaces in all tests was boehmite.

Metallographic Examination. At least three, and sometimes five, transverse sections of one axial half of each specimen were mounted in Bakelite, polished, etched, and examined microscopically. In all those cases where film stripping

had not occurred, except test A-17, a reasonably uniform oxide coating firmly attached to the base metal was observed. Figure 10 shows four sections from different specimens and shows the oxide on the aluminum surface as well as the very uniform nature of the attack on the metal. In every section prepared where film stripping had not occurred, again excepting test A-17, the metal had undergone only a uniform surface attack; in no case was even a hint of localized attack of any kind observed. The oxide on the surface of the specimen frequently showed cracks but the oxide adhered well to the metal. Whether all the cracks formed during the test or were produced during preparation of the specimen for examination cannot be definitely established; but in view of the observation that at least some cracks originated as a result of slight heating of the specimen, it is probable that most of them formed after the test.

As shown in Fig. 3, the temperature-time curves for test A-17 were unusual, but the surface appearance of the specimen at the end of the test was normal; there was no evidence of film stripping. Examination of the metallographically polished sections from the specimen, however, showed random pits in the aluminum in contrast to all other specimens. In addition to each pit being full of oxide, a mound of oxide extending above the surface of the pit was present at most pit locations. Figure 11 illustrates such a pit. Why test A-17 behaved in an abnormal manner is not known. It should be noted that tests A-18, A-19, and A-20 were run under similar conditions, and no evidence of localized attack or unusual temperature behavior was observed in these tests.

On each metallographic section examined, except those in film-stripped regions, the oxide thickness on the 0.1-in.-thick section of the specimen (the region subjected to the high heat flux) was measured. Up through test A-14 the minimum and maximum oxide thicknesses were measured microscopically in six equal intervals across the 0.3-in.-wide center portion of the specimen. These 12 measurements were averaged to determine the oxide thickness at that particular axial location. In tests after A-14, the 12 measurements were similarly made except that in these cases they were limited to the 0.1-in.-wide interval located in the transverse

T19597

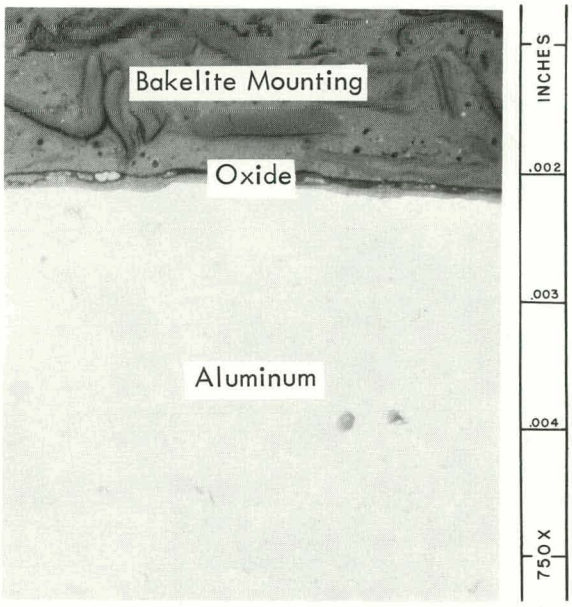

Specimen A-13, 3 1/4 in. from Outlet

T19745

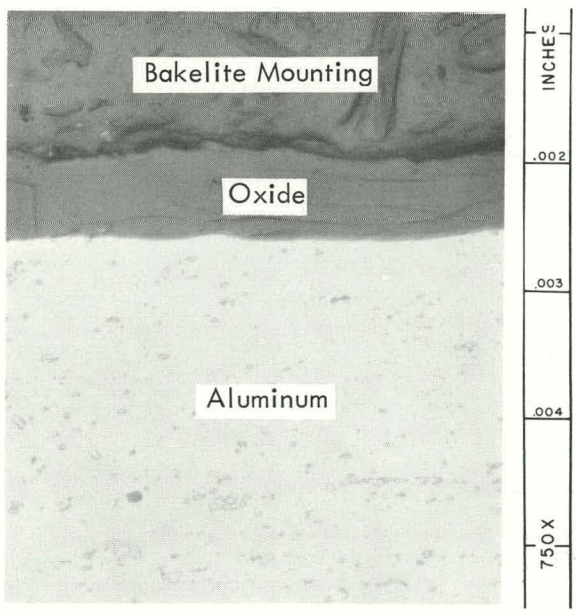

Specimen A-16, 1 in. from Outlet

T20107

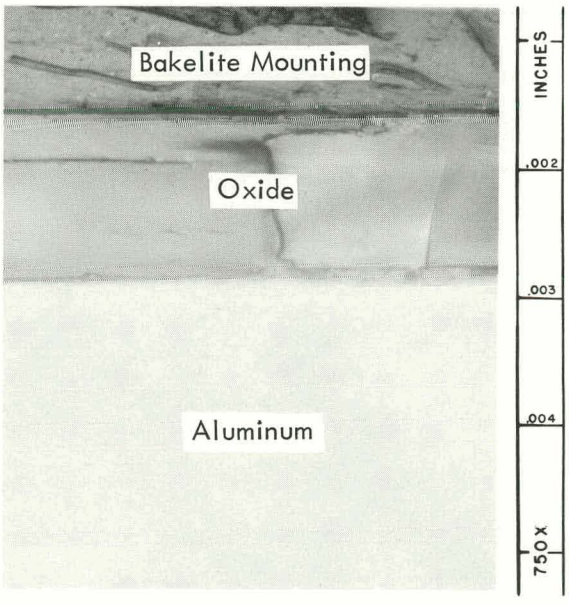

Specimen A-20, 1 in. from Outlet

T20209

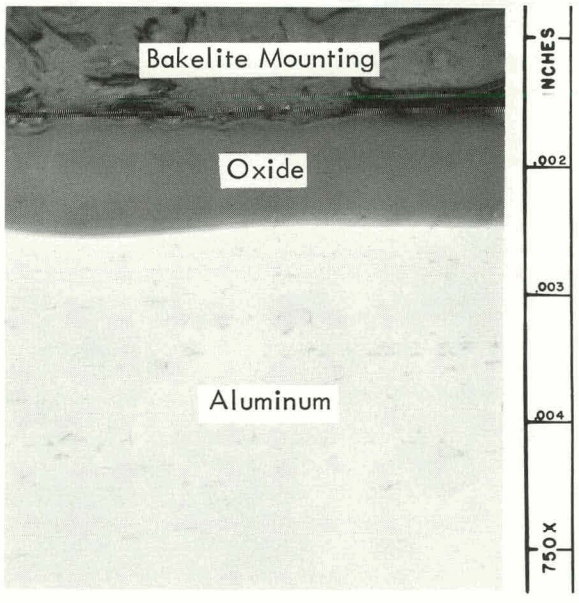

Specimen A-24, 1 in. from Outlet

Fig. 10. Cross-Sectional View of Four Specimens Showing Oxide Film and Uniform Corrosion of Aluminum.

center of the specimen. There were actually only slight differences in the results obtained by the two methods, and in measuring the oxide thicknesses on several sections both ways it appeared that the latter method gave oxide thickness no more than 5% greater than by the former method. Table 4 shows the measured oxide thicknesses.

T19741

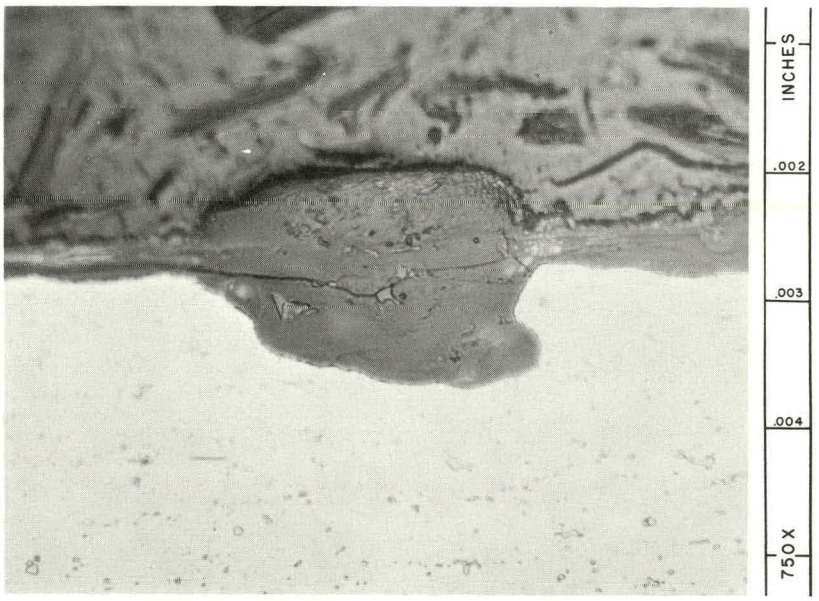

Fig. 11. A Photomicrograph of a Pit Found on Specimen A-17. Section Taken 6 1/4 in. from Outlet.

In every case where film-stripping occurred, localized attack of the underlying aluminum was observed. Figure 12 shows an enlarged photograph of a transverse section near the outlet of specimen A-23 which represents the most severe case of stripping encountered, and Fig. 13 shows a further enlargement of the corroded area in the center of the specimen. The voids in the metal and the complete encirclement of particles of metal by oxide are similar to those observed after exposing aluminum to high-temperature water in isothermal tests.[7] Figure 14 is a photomicrograph showing the localized attack found in the film-stripped region in test A-21 where the attack was less extensive.

Table 4. The Corrosion-Product Thickness Determined Microscopically from Metallographically Polished Sections

Test No.	Average Corrosion-Product Thickness (mils) Distance from Inlet End of Specimen (inches)											
	0.25	1.00	1.25	2.00	3.00	3.25	3.50	4.00	5.00	5.25	5.50	6.00
A-2		0.73		1.13	1.76			1.86	1.46			
A-3		0.70		0.85	0.84			1.10	1.17		1.20	
A-6		0.98		1.24	1.66			1.66	1.78			1.39
A-7		0.30		0.30	0.41			0.40	0.36			0.61
A-8		0.15					0.30					0.43
A-9		0.44					0.49					0.74
A-11		0.26					0.43					0.51
A-12	0.15					0.24				0.26		
A-13			0.09			0.13					0.17	
A-14		0.29				0.47					0.38	
A-16		0.48				0.80					0.83	
A-17	0.49					0.36						0.53
A-18		0.68		0.82		0.98		1.17*			1.38	
A-19			0.61			0.60				0.56		
A-20		0.73				1.09					1.36	
A-21			1.43			1.67						
A-22		0.21				0.29					0.33	
A-23		1.13										
A-24		0.66				0.76					1.11	

*Measurement made 4.5 in. from inlet.

Film-stripping was not observed in any of the tests in which the pH of the water was controlled at 5.0 or 5.3. However, it is probable that the lack of stripping under these conditions was related to the fact that oxide formed at a low rate, and during the 10-day test period the oxide did not reach sufficient thickness. Stripping was only observed when oxide thicknesses were considerably greater than 1 mil. If the actual thickness of the oxide is important and if the oxide thickness increased in a linear fashion, then all specimens would have

T20202

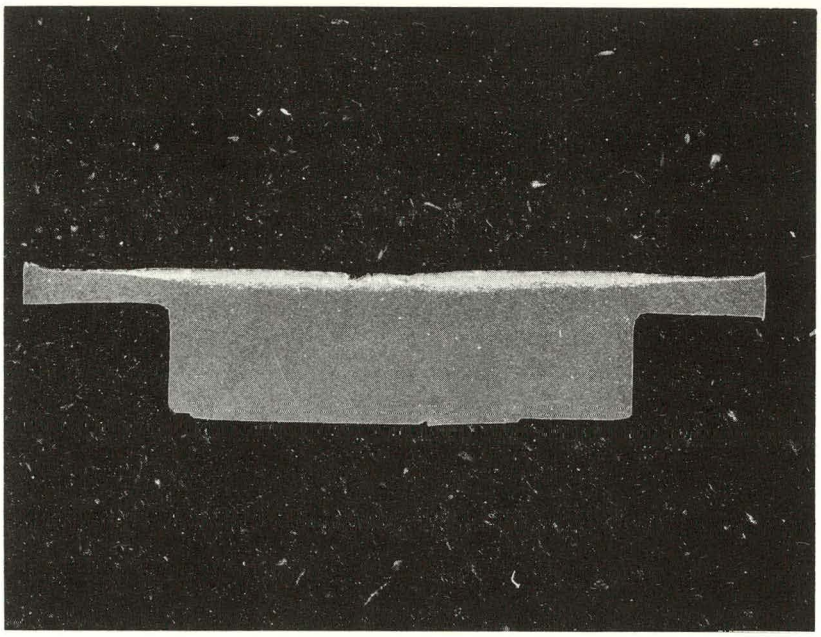

Fig. 12. A Photograph of a Transverse Section of Specimen A-23 Illuminated by Oblique Light. Section Taken 1 in. from Outlet. (Magnification 9X)

T20204

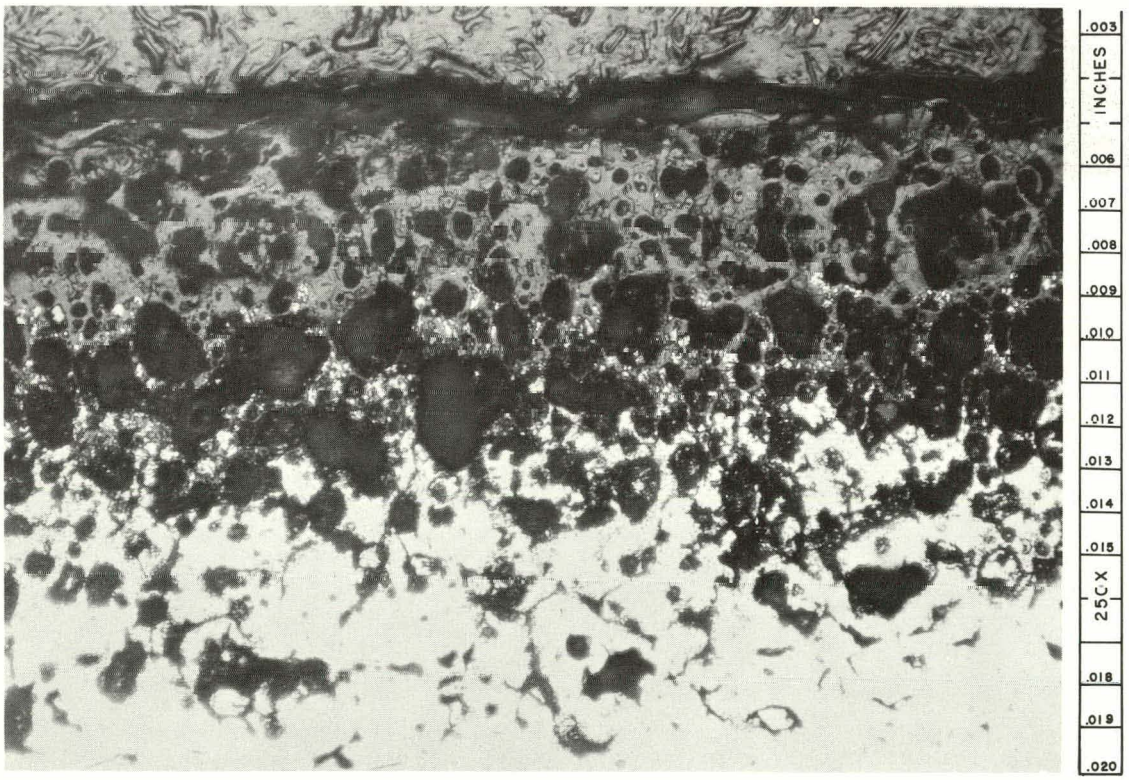

Fig. 13. A Photomicrograph of the Corroded Area in Test A-23. Location 1 in. from Outlet.

T20108

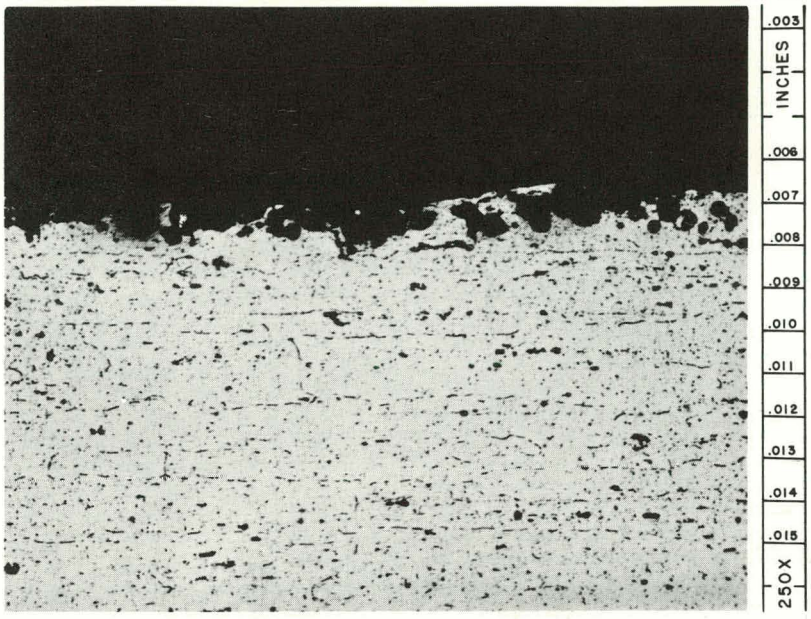

a. Photographed to show microstructure of metal.

T20109

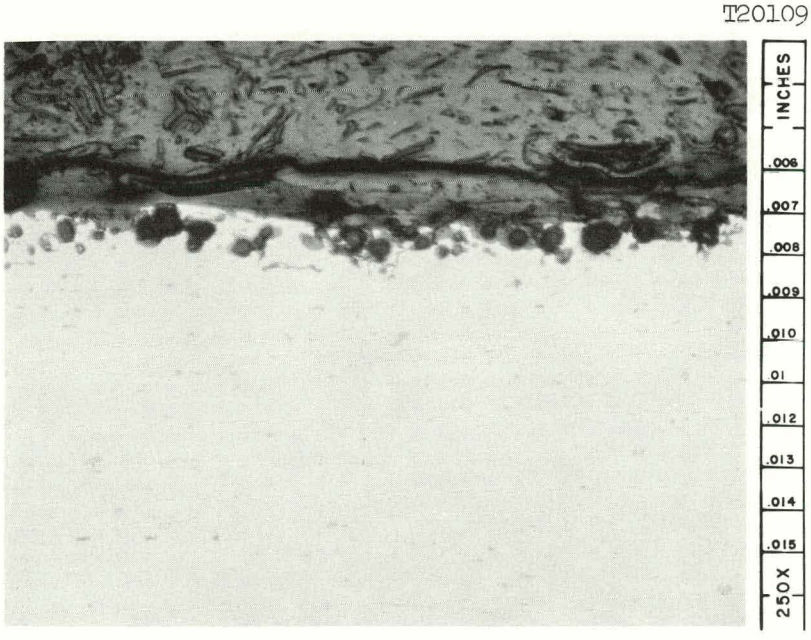

b. Photographed to show oxide on surface.

Fig. 14. Photomicrographs of the Same Section of Specimen A-21 Showing Localized Attack. The Section was Taken 1/2 in. from Outlet.

undergone stripping had the tests been conducted long enough. This point was not checked in the experimental program.

Corrosion Penetration. For all tests through A-13 the specimen was fabricated from a drilled rod, and with this type of specimen quantitative corrosion information was not obtained. Visual examination of the specimens at the end of these tests, however, indicated that corrosion damage was not excessive except in test A-2 where film-stripping and localized attack had occurred.[4]

Quantitative corrosion penetration measurements were obtained from all specimens in tests subsequent to A-13 except specimen A-23, which was also fabricated from a drilled rod. Before each specimen was assembled, the thickness of each half was determined in the center at several specific axial locations with a precision micrometer. At the conclusion of the test the oxide film was removed from the specimen (except for those sections mounted for metallographic examination), and the specimen thicknesses were determined at exactly the same locations as before the start of the test. Table 5 shows the penetrations observed. The two sides of the specimens were arbitrarily designated A and B, and the A and B columns refer to the measurements on the two sides. In those cases where film-stripping occurred, it was not possible to remove the oxide completely or to measure the localized penetrations accurately (see Fig. 13), and therefore corrosion penetrations in those few cases are of questionable accuracy. Although data for test A-17 are included in Table 5, it should be remembered that localized pitting occurred and this is not included in the measurements in the table.

Examination of Table 5 reveals several general trends in the data. In any one test the agreement between the measured penetrations on each half of the specimen was reasonably good. In most cases the extent of penetration was greater toward the outlet end of the specimen than at the inlet end. Since the bulk water and surface temperatures increased from inlet to outlet, this observation was expected. Similarly, the average penetration from run to run was usually greater the higher the surface temperature (see Table 1).

Table 5. Corrosion of the Aluminum Test Specimens

Distance from Inlet (in.)	Corrosion Penetration (mils)																	
	A-14		A-16		A-17		A-18		A-19		A-20		A-21		A-22		A-24	
	A	B	A	B	A	B	A	B	A	B	A	B	A	B	A	B	A	B
0.50	1.0	0.9	0.5	0.8							0.2	0.3	0.7	0.8	0.2	0.1	0.6	0.5
0.75					0.3	0.1	0.4	0.1	0.8	0.7								
1.00	0.5	0.5	-	0.1							0.2	-	-	1.1	-	0.5	-	0.7
1.25					0.2	-	0.5	0.5	-	0.8								
1.50	0.5	0.4	0.1	0.2							0.2	0.4	0.8	0.9	0.1	0.2	0.9	0.8
1.75					0.3	0.2	0.6	0.7	0.1	0.4								
2.00	0.3	-	0.3	0.3							0.6	0.5	0.7	0.9	0.1	0.1	0.8	0.8
2.25					0.3	-	-	0.8	0.6	0.7								
2.50	0.5	0.3	0.4	0.4							0.5	0.6	0.7	0.7	0.3	0.2	0.7	0.8
2.75					0.4	0.3	0.7	0.8	0.3	0.5								
3.00	0.6	-	0.2	0.4							0.7	0.7	0.8	1.0	0.2	0.3	0.8	0.8
3.25									0.5	0.5								
3.50	0.8	0.6	0.4	0.2	0.2	0.3					0.8	0.8	0.7	1.1	0.2	0.2	0.8	1.0
3.75					0.2	0.3	0.4	1.0	0.5	0.5								
4.00	0.5	0.7	0.4	0.2							1.0	0.9	0.8	1.0	0.3	0.3	0.9	0.9
4.25					0.2	-	-	1.0	0.5	0.5								
4.50	0.4	0.5	0.3	0.3							1.1	1.0	1.0*	1.2*	0.3	0.4	0.9	1.0
4.75					0.2	0.3	0.7	0.9	-	0.6								
5.00	0.4	0.5	0.2	0.3							1.1	1.2	1.4*	1.1*	0.5	0.6	0.6	0.6
5.25					0.2	-	-	1.0	0.8	0.8								
5.50	1.1	-	-	0.5							1.3	-	-	1.5*	-	0.6	-	-
5.75					0.5	0.2	3.9**	1.4	-	1.1								
6.00	1.1	1.3	0.4	0.5							1.5	1.4	-	1.0**	0.5	0.5	0.3	0.6
6.25					0.2	-			1.0	1.1								

*Corrosion product probably not completely removed.
**Probably in error.

Tests A-14 and A-16 were conducted under similar conditions except in the latter run the heat flux was somewhat greater and the run lasted twice as long. It can be noted from Table 5 that the extent of corrosion was greater in A-14 than in A-16 although the reverse was expected. At this time there is no explanation for this observation. The rate at which the temperature of the specimen increased with time was essentially the same in the two runs, and the oxide was about twice as thick on specimen A-16 as A-14, as one would predict.

With the exception of test A-16 where the oxide thickness was about a factor of 2 greater than the metal loss, the thickness of metal corroded was roughly equal to the thickness of the corrosion-product film. Comparison of Table 4 (oxide thickness) with Table 5 (metal loss) shows that the above statement was generally true although rather wide variations were observed. This same general relationship was observed in isothermal tests conducted in the temperature range of 170 to 230°C (338 to 446°F) and in the velocity range of 31 to 44 fps.[7] If one assumes that the density of the corrosion product is 3.02 g/cm^3 as reported by Ervin and Osborn[10] for boehmite, then for each mil of aluminum corroded, 2 mils of corrosion product would be formed. Thus the data tabulated in Tables 4 and 5 as well as that previously reported indicate in very general terms that only about half of the corrosion product remained on the surface.

Heat-Transfer Considerations

Temperature measurements obtained from thermocouples attached to the outside surface of the specimens, along with the coolant flow rates, coolant inlet and outlet temperatures, specimen dimensions, and electrical and thermal conductivities of the aluminum alloys were used to calculate the fluid-film heat-transfer coefficients from the experimental data. These coefficients are compared with values obtained from conventional empirical equations and with the experimental values reported by Gambill and Bundy.[11]

In addition to the fluid-film heat-transfer coefficients, sufficient data were obtained to calculate values for the thermal conductivity of the corrosion-product layer formed on the water-cooled specimen surfaces.

Treatment of Data. The specimen was heated by passing an electric current through it and heat was removed by water flowing through the rectangular-shaped flow channel. The total power input was determined from both the electrical power and the cooling-water heat balance, and as previously reported[4] these two values were usually in excellent agreement with the electrical heat input slightly higher than the heat removed by the cooling water. This was expected because of small heat losses other than to the cooling water. The water heat balance was used in all cases to regulate and control the heat input since this value more nearly represented the heat actually transferred across the water-cooled specimen surface. Heat fluxes were calculated from the cooling-water heat balance considering that 80% of the total heat was transferred across the specimen surface under the 0.100-in.-thick portion of the specimen (refer to Fig. 1).

Calculation of the fluid-film heat-transfer coefficients and thermal conductivities of the corrosion products from the experimental data involved the following assumptions:

1. The water-cooled surface of a specimen was free of corrosion products at the start of a test.

2. All dimensions of the specimens were as shown in Fig. 1 and did not change during test.

3. At any axial location heat was generated uniformly through the thickness of the specimen wall.

4. The electrical and thermal properties of the aluminum throughout the thickness of the specimen at any point were determined by the temperature indicated by a thermocouple on the outside surface of the specimen at that point.

5. The fluid-film heat-transfer coefficient, h, at a given location remained constant throughout the test.

6. The bulk water temperature increased uniformly from inlet to exit in passing through the heated section.

The temperature dependence of the thermal conductivity and electrical resistivity of 1100 and 6061 aluminum are shown in Fig. 15. These data were supplied by the Aluminum Company of America.[12] From the data in Fig. 15 and from a knowledge of the total heat transferred across the specimen surface (80% across the thick part of the specimen), local heat fluxes at points corresponding to each thermocouple location were calculated at the beginning and the end of each run (see appendix for calculational method).

At the beginning of each test the temperature drops (Δt) across the specimen wall and the fluid film were calculated at points corresponding to the thermocouple locations. The Δt across the specimen wall was determined from the local heat flux and the thermal conductivity of the aluminum at that point. The Δt across the fluid film was calculated by subtracting the metal wall Δt and the bulk coolant temperature from the temperature indicated by the thermocouple attached to the outside surface of the specimen. The local fluid-film heat-transfer coefficient was then obtained by dividing the local heat flux at each point by the fluid-film temperature drop at the corresponding point.

The thermal conductivity of the corrosion-product layer was calculated from the measured oxide thickness (values shown in Table 4), the Δt across the oxide, and the local heat flux determined at the end of the test. To obtain the Δt across the oxide, the metal wall Δt, fluid-film Δt, and coolant temperature were subtracted from the temperature indicated by the thermocouple on the outside surface of the specimen at the end of the run. In this case the metal wall temperature drop was calculated from the local heat flux existing at the end of the test, and the fluid-film temperature drop was calculated from the final local heat flux and the fluid-film heat-transfer coefficient obtained at the beginning of the test (assumed constant throughout the run).

The procedures and equations used in calculating the heat-transfer data are given in the appendix along with definitions of all terms and symbols.

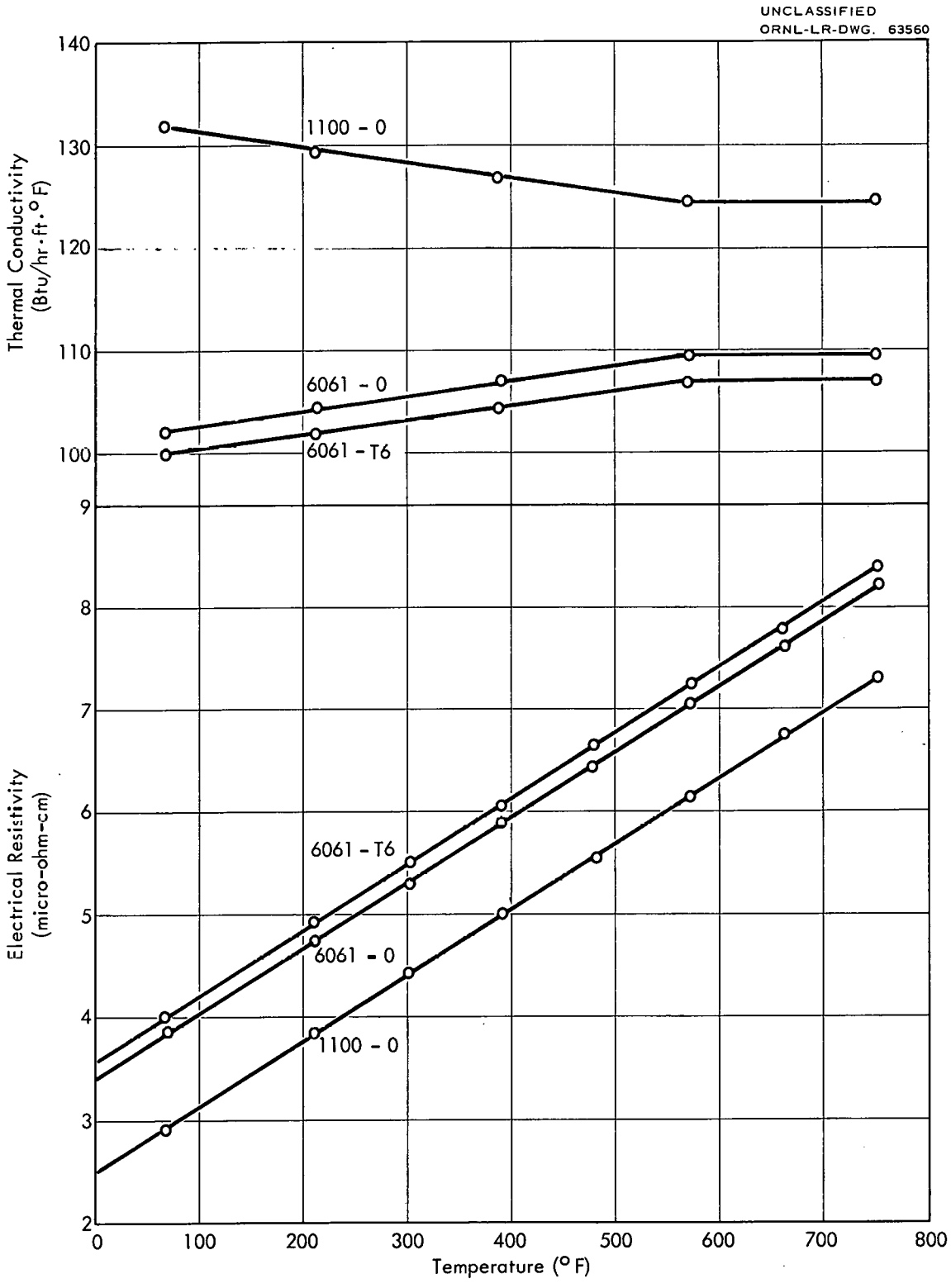

Fig. 15. Electrical Resistivity and Thermal Conductivity of Aluminum Alloys

The data for tests A-13 and A-17 are not included in this section. Not only was corrosion abnormal in test A-17, but as previously noted, the specimen temperature at the start of the test was also abnormal. Using the experimental values, unusually low fluid-film heat-transfer coefficients would have been calculated. Normal fluid-film heat-transfer coefficients were obtained from test A-13, but using the method of obtaining oxide thermal conductivity outlined above, thermal conductivity values equal to zero or even slightly negative would have resulted. In test A-13 the thinnest oxide films formed on any specimen were observed. Thus the temperature drop over the oxide was very small compared with the drop over the fluid film, and it was not surprising that meaningful values of thermal conductivity could not be obtained by the above method of calculation.

Fluid-Film Heat-Transfer Coefficients. Experimental fluid-film heat-transfer coefficients, h, for 17 test specimens (56 points) are given in Table 6. Figure 16 is a standard log-log plot of a function of h versus Reynolds number and includes the data from this investigation as well as that of Gambill and Bundy.[11] The excellent agreement between the two sets of data is apparent. It should be noted that the Gambill and Bundy points represent the average over their entire test specimen for a given run, while the points from this study represent local values at definite points. This indicates that h values based on bulk coolant properties and average interface temperatures would not be greatly different from local h values at a given point. The line appearing on the plot represents the standard Sieder-Tate equation,[13]

$$\left(\frac{h\,D_e}{k}\right)_{bm} = 0.027 \left(Re\right)_b^{0.8} \left(Pr\right)_b^{0.33} \left(\frac{\mu_b}{\mu_w}\right)^{0.14} .$$

Nearly 21% of the coefficients calculated from the data of this study lie below this line; however, only 6% of the points would lie below the line if the Sieder-Tate coefficient were reduced from 0.027 to 0.024 as suggested by Gambill and Bundy.

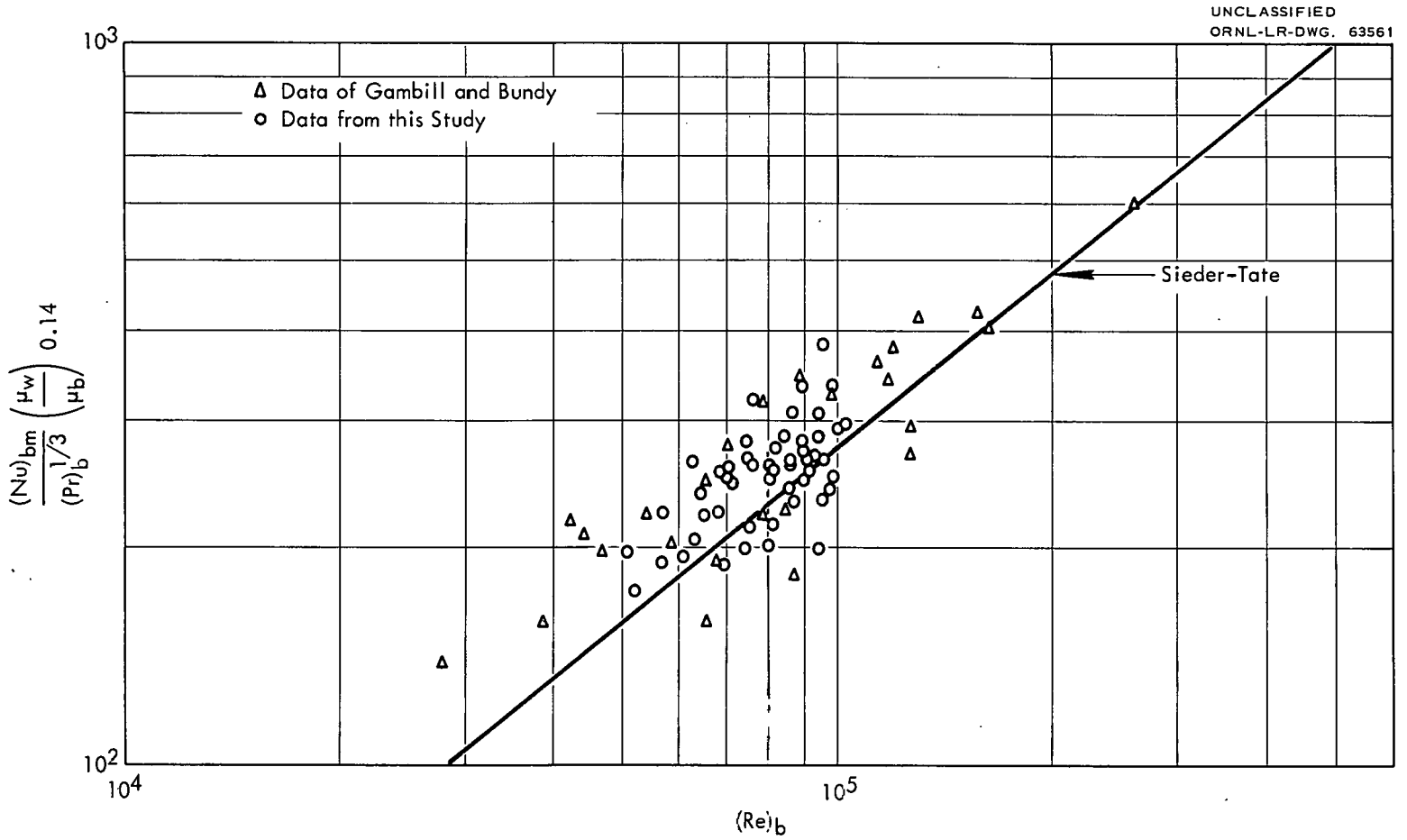

Fig. 16. Comparison of Experimental Local Heat-Transfer Coefficients with Sieder-Tate Correlation and with Average Values for Thin Rectangular Channels Obtained by Gambill and Bundy.

Table 6. Experimental Heat-Transfer Data

Test No.	Distance from Inlet End (in.)	Local Heat Flux[a] (Btu/hr·ft²) x 10^{-6}	Coolant Flow Rate (fps)	Coolant Temp. (°F) Inlet	Coolant Temp. (°F) Outlet	Reynolds Number	ΔT (°F)[a] Oxide	ΔT (°F)[a] Fluid Film	k (Btu/hr·°F·ft²/ft)	h (Btu/hr·ft²·°F)
2	1.00	1.64	41	152	189	68,800	62	112	1.6	14,600
	2.25	1.69				-	79	109	2.0	15,500
	3.25	1.76				75,800	103	110	2.6	16,000
	4.25	1.83				-	128	111	2.2[b]	16,500
	5.50	2.01				80,600	174	137	1.4[b]	14,700
3	1.00	1.61	37	151	190	63,200	84	105	1.1	15,400
	1.25	1.64				-	88	115	1.3	14,200
	3.25	1.70				68,500	111	104	1.1[b]	16,400
	4.25	1.80				-	134	120	1.2[b]	15,000
	5.50	1.89				74,600	158	131	1.2[b]	14,400
6	1.00	1.59	38	153	193	-	97	85	1.3[b]	18,800
	2.25	1.67				68,600	121	90	1.4[b]	18,700
	3.25	1.75				71,300	144	94	1.7[b]	18,700
	4.25	1.78				-	159	86	1.5[b]	20,800
	5.25	1.84				76,700	185	82	1.5[b]	22,500
7	1.00	1.55	38	157	194	65,400	24	90	1.6	17,200
	2.25	1.56				-	26	87	1.5	18,000
	3.25	1.60				71,500	32	91	1.7	17,600
	4.25	1.62				-	32	92	1.7	17,500
	5.25	1.66				76,200	46	90	1.1	18,400
8	1.00	1.56	37	154	191	64,600	23	85	0.8	18,500
	3.25	1.61				69,500	30	87	1.3	18,500
	5.50	1.67				74,400	44	82	1.4	20,400
9	1.00	1.51	35	186	227	74,300	40	82	1.4	18,600
	3.25	1.57				80,400	51	79	1.3	19,700
	5.50	1.66				86,200	64	94	1.6	17,600

11	1.00	1.46	33	153	195	52,300	20	112	1.6	13,000
	3.25	1.49				56,900	23	111	2.3	13,400
12	3.25	1.51	51	166	193	97,900	14	68	2.3	22,300
	5.25	1.56				102,800	30	69	1.1	22,600
14	1.25	1.32	40	190	220	85,800	29	74	1.1	18,000
	3.25	1.36				90,700	41	76	1.3	17,900
	5.50	1.40				95,600	51	80	0.9	17,600
16	1.00	1.56	41	185	219	84,600	62	71	1.0[b]	22,100
	3.25	1.59				90,200	72	71	1.5[b]	22,500
	5.50	1.65				95,200	87	72	1.3[b]	22,900
18	1.00	2.03	41	174	219	81,500	58	129	2.0	15,800
	2.25	2.05				-	68	116	2.1	17,600
	3.25	2.14				87,700	87	131	2.0	16,300
	4.25	2.20				-	107	131	2.0	16,800
	5.50	2.33				95,500	137	145	2.0	16,000
19	1.00	1.79	41	179	218	80,400	59	94	1.5	19,200
	3.25	1.81				87,100	65	82	1.4	22,300
	5.25	1.90				93,800	91	87	1.0[b]	21,800
20	1.00	1.84	42	181	218	86,100	90	111	1.2[b]	16,600
	3.25	1.93				93,000	125	108	1.4[b]	17,800
	5.50	2.06				99,400	177	110	1.3[b]	18,800
21	1.25	1.99	41	176	220	82,300	159	102	1.5[b]	19,500
	3.25	2.08				89,100	204	91	1.4[b]	22,800
22	1.00	0.96	41	198	219	90,200	7	58	2.4	16,600
	3.25	0.99				94,700	13	75	1.8	13,300
	5.50	0.98				98,000	12	62	2.2	16,000
23	1.00	1.96	41	175	218	-	223	109	0.8[b]	18,000
24	1.00	1.62	37	210	250	89,700	48	89	1.9	18,300
	3.25	1.68				94,800	73	95	1.5[b]	17,700
	5.50	1.77				100,900	105	95	1.6[b]	18,700

[a] These values were calculated from conditions existing at the end of the run.
[b] For these values of k, the temperature drop over the oxide film approximately equaled or exceeded the temperature drop over the fluid film.

Figure 17 is a similar plot which compares the local fluid-film heat-transfer coefficients obtained in this study with the local values of Gambill and Bundy. The straight line shown here represents the local h predicted by the Hausen equation[14] as modified by Gambill[11] for determination of local h values,

$$\left(\frac{h\,D_e}{k}\right)_{bx} = 0.116\left[\left(Re\right)_{bx}^{2/3} - 125\right]\left(Pr\right)_{bx}^{1/3}\left[1 + \frac{1}{3}\left(\frac{D_e}{x}\right)^{2/3}\right]\left(\frac{\mu_b}{\mu_w}\right)^{0.14}.$$

Less than 5% of the h values calculated from the data fall below that predicted by the Hausen equation. The Hausen equation for average h values with the coefficient of this equation reduced by 6% from 0.116 to 0.109 was recommended as the design criterion for calculating average h values under HFIR conditions.[11]

Thermal Conductivity of the Corrosion-Product Film. The thermal conductivity values, k, of the corrosion-product film ($\alpha Al_2O_3 \cdot H_2O$) as calculated for 56 points are presented in Table 6. The average value of k for all points was 1.5 Btu/hr·ft^2·°F/ft. There appeared to be no correlation of k with the oxide temperature over the range of temperatures encountered.

The average value for k, determined to be 1.5 for all runs, had a standard deviation of 0.4, or 27%. A satisfactory explanation for such a large standard deviation can be made on the basis that a 15% variation in h, which is about the average in many tests, introduces a 15% variation in the calculated fluid film temperature drop. This will cause a varying percentage error in the calculated temperature drop across the oxide which, in turn, results in a varying percentage deviation in the value calculated for the thermal conductivity of the oxide.

The magnitude of possible error or percentage deviation in k will depend upon the relative magnitude of the temperature drops calculated for the fluid film and for the oxide. This is demonstrated by Fig. 18 which shows that a ±10% error in the calculated k is possible only when the calculated temperature drop across the oxide is more than twice the apparent drop across the fluid film, providing that the deviation in h is ±15%. Clearly the deviation in k caused by a 15% deviation in h is less than 17.5% for all cases where the oxide temperature drop exceeds the fluid-film temperature drop. This suggests that a better average value for k

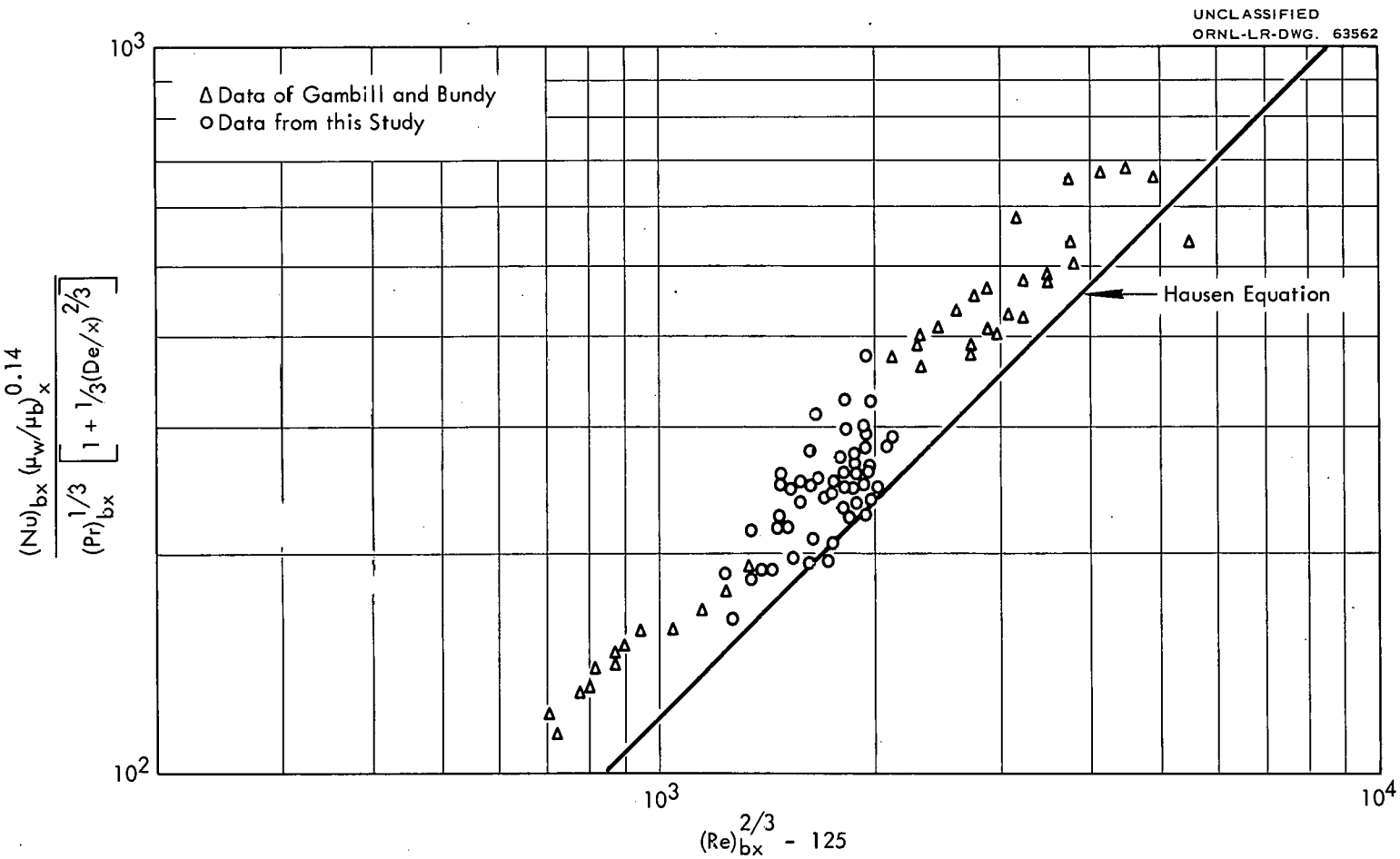

Fig. 17. Comparison of Experimental Local Heat-Transfer Coefficients with Hausen Correlation and with Local Values for Thin Rectangular Channels Obtained by Gambill and Bundy.

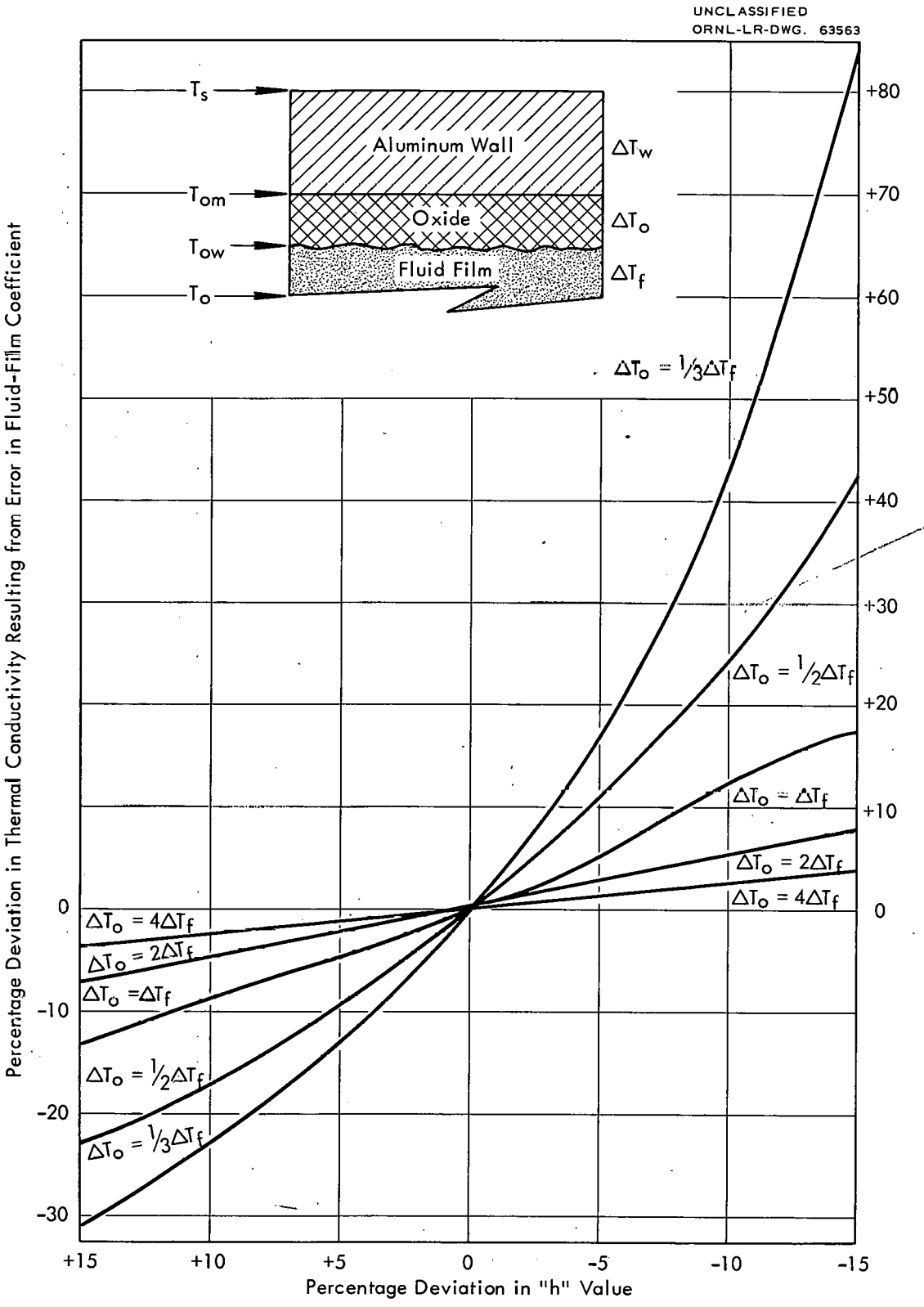

Fig. 18. Error in Calculated Thermal Conductivity Caused by Error in Fluid-Film Coefficient.

might be obtained by considering only those runs which had oxide temperature drops exceeding the fluid-film temperature drop.

For the values of k shown in Table 6, the 21 values marked with an asterisk meet this criterion or closely approach it. The average k for this group was 1.3, with a standard deviation of 0.2, excluding the two extreme values of 0.8 and 2.2. This corresponds to a deviation of $\pm 15.4\%$ in the selected k values. On this basis 1.3 ± 0.2 is considered the best value for the thermal conductivity of the corrosion-product layer formed during these tests.

DISCUSSION AND CONCLUSIONS

As a result of this study it appears that either 1100 or 6061 aluminum has adequate corrosion resistance for use as cladding material in the HFIR provided the pH of the coolant is adjusted to 5.0 or 5.3 with nitric acid. Although most of the tests conducted in this program lasted only 10 days, the greatest penetration observed when the pH of the coolant was 5.0 or 5.3 was 1.5 mils, even when the heat flux was slightly greater than 2×10^6 Btu/hr·ft^2 (except for one case where the value was 3.9 mils, a measurement probably in error). Test A-24 was conducted under conditions slightly more severe than expected in the HFIR (hot spot - hot channel condition), and the deepest penetration observed was only 1.0 mil during the 10-day test. If the assumption is made that the corrosion rate was constant during the 10-day period and would continue to remain so, the total penetration would be 1.5 mils during 15 days, the approximate life of an HFIR core. Since the minimum design cladding thickness for the HFIR fuel elements is 10 mils, a penetration of only 15% of the cladding under conditions even more severe than anticipated in the reactor does not seem unreasonable.

On the other hand, it is doubtful if either 1100 or 6061 aluminum would be suitable cladding materials for the HFIR fuel elements if pure water were the coolant. In view of the localized attack encountered on both alloys when the coolant was deionized water, it is probable that near or total penetration of the clad would occur at the hot spots during a reactor cycle. In addition,

oxide thicknesses on the remainder of the surfaces would likely be great enough to produce excessive fuel-element temperatures. Aluminum and most of its alloys have poor strength properties even at room temperature, and the mechanical properties of all the alloys become less favorable as the temperature increases.[15] Thus the addition of acid to the coolant has two related effects: (1) the direct effect of minimizing fuel-element corrosion damage, and (2) the indirect effect of minimizing fuel-element temperatures.

Because of the strength factor, the 6061 aluminum alloy is the reference alloy for the HFIR fuel cladding. At the temperatures of interest in the HFIR, both the yield strength and creep resistance of the alloy, even in the annealed state, are superior to those of the 1100 alloy.[15] In the hardened condition (T-6) the mechanical properties of the alloy are even more favorable and corrosion resistance is equal to that in the annealed condition; but mechanical difficulties in forming the fuel plates preclude the use of the alloy in the T-6 condition.

From the standpoint of reactor operation, it is simpler to use deionized water as a coolant than to acidify the water. However, it has been shown by other investigators,[8,9,16] as well as demonstrated in this study, that at high temperatures the corrosion rate of aluminum is less in acidified water than in pure water. To achieve the high performance expected in the HFIR, it appears necessary to acidify the water. Although only nitric acid was used in this investigation, its effect was marked and its use in the HFIR should give adequate performance. Phosphoric acid has been shown to be a better inhibitor than nitric acid,[16,17] but the practicability of using this acid in a high-flux reactor is questionable. Not only would the phosphorus in the acid produce unwanted activities in the reactor system, but the problem of controlling the pH of the coolant with an acid that forms insoluble salts with practically all cations originating from corrosion of the structural material in the system would be difficult. Since nitric acid presents no problems with activation and forms no insoluble salts, and since its concentration can be easily controlled with cation and/or mixed-bed

ion exchangers, its use to lower the pH of the water in the HFIR is less objectionable than would be the use of any other acid.

No measures of the incremental corrosion rate of aluminum during the 10-day tests were obtained in this investigation, but it appeared that the corrosion products that adhered to the aluminum surface formed at a constant rate during a test although only about half of the aluminum oxidized adhered to the specimen. If it is assumed that the corrosion rate was constant during a test, the results are somewhat surprising. Other investigators have noted that when aluminum through which heat is being transferred is corroded it is the temperature at the aluminum - aluminum-oxide interface[18] or the average temperature in the oxide layer[19] that determines the corrosion rate. In this study both of these temperatures increased substantially during a test, and yet the rate of oxide accumulation on the aluminum was constant. It has been shown that the rate of oxide buildup was related to the temperature at the aluminum oxide - water interface. In fact, when the data are presented on an Arrhenius-type plot, the data points fit a straight line reasonably well. Since it has not been established that the rate of oxide accumulation on the aluminum is directly proportional to corrosion rates in this particular case, the fundamental significance, if any, of the straight-line relationship is not clear; however, the correlation provides a reasonable means of estimating the rate of oxide buildup on aluminum surfaces under conditions approximating those for the HFIR. It should be noted that oxide thickness would not increase indefinitely, and eventually some sort of a limiting thickness would result. Therefore the correlation could not be used to estimate fuel-element temperatures in cases where oxide sloughed or spalled from the surface as was observed in some of the runs with deionized water. Furthermore, it should be noted that the data presented in this report were obtained under very high heat-flux conditions in a rather narrow range of flow rates. Whether the correlation would be applicable at lower heat fluxes and higher coolant temperatures (to produce surface temperatures in the same range as those investigated) remains to be demonstrated. Certainly the

correlation would not be expected to be valid at flow rates substantially different from those used in this investigation.

An important variable in the corrosion of aluminum by flowing water is the ratio of exposed aluminum surface area to the volume of water in the system. It has been shown by several investigators[16,17,20] that if the ratio is large, lower corrosion rates are observed than if it is small. For example, in isothermal tests in which aluminum was exposed to water flowing at 18 fps for one week, Draley et al.,[17] showed specimen weight losses of 9.8 mg/cm^2 when the ratio was 2 cm^2/liter and 7.6 mg/cm^2 when the ratio was 20 cm^2/liter. In this test program the area/volume ratio was 1.85 cm^2/liter, and in the HFIR the ratio will be 7 cm^2/liter. Interpolating from the curve of Draley et al.,[17] and assuming that the effect in heat throughput tests at flow rates higher than employed by Draley is the same as in his isothermal tests, corrosion in the HFIR would be about 15% less than predicted from the tests conducted in this program.

The effect of reactor radiation on the corrosion of aluminum was not considered in this investigation, but from information reported in the literature[16,18,21] it is not expected that radiation will have a significant effect on the corrosion process. Both the Materials Test Reactor and the Engineering Test Reactor use aluminum-clad fuel elements, and although the fluxes are lower in these two reactors than in the HFIR, no detrimental effect of radiation on corrosion has been reported.

The thermal conductivity of the corrosion-product layer obtained by averaging all of the experimentally determined values is 1.5 $\pm$ 0.4 Btu/ft^2·hr·°F/ft. Using select values for reasons discussed in a previous section, a value of 1.3 $\pm$ 0.2 Btu/hr·ft^2·°F/ft is obtained. Although the two values are within the same range, the latter value is believed to be nearer the true thermal conductivity than the former. The value of 1.3 Btu/hr·ft^2·°F/ft also agrees well with the value of 1.4 obtained by analysis of empirical data acquired at Hanford.[16]

In a previous report[5] which included a part of the data presented in this report, a value of 1 Btu/hr·ft^2·°F/ft was given. This value was obtained from the slope of the line fitted to the points on a temperature drop versus oxide

thickness plot, assuming all tests were conducted at a heat flux of 1.5×10^6 Btu/hr·ft^2. More recent analysis of the experimental data shows that in these tests the heat flux varied somewhat from run to run and that in all cases the heat flux was greater than 1.5×10^6 Btu/hr·ft^2 (see Table 1, tests A-2 through A-13). This fact, combined with the data acquired from additional tests, accounts for the different value presently reported.

It has been calculated that the maximum surface temperature to be expected in the HFIR is 344°F.[3] Using the data presented in Fig. 6, it is estimated that the oxide thickness developed during a 15-day exposure would be 2.1 mils. Assuming that the heat flux was constant at 1.52×10^6 Btu/hr·ft^2 for the core lifetime and that the thermal conductivity of the oxide is 1.3 Btu/hr·ft^2·°F/ft, the temperature drop across the oxide would be 205°F. Thus at the end of the test, the temperature at the aluminum - aluminum-oxide interface would be 549°F. Although this temperature is higher than one would like, this value is probably tolerable, particularly in view of the fact that this is a condition that would be expected to exist only very rarely on only a very small area. Certainly penetration of the clad would not be expected if the pH is properly controlled, and the area of the clad involved would be too small to have an effect on the plate stability. Evidence that penetration of the clad would not be expected was provided by test A-24 in which the surface temperature was 337°F near the outlet of the specimen and the penetration did not exceed 1 mil in 10 days.

Eliminating hot-spot considerations, the maximum fuel-element surface temperature is calculated to be 307°F and the heat flux, 1.32×10^6 Btu/hr·ft^2.[3] Making the same assumptions as above, only 1.02 mils of oxide would be expected, and this would result in a temperature drop over the oxide of 86°F. Thus the temperature at the aluminum - aluminum-oxide interface would be only 393°F.

Although this experimental program was not able to duplicate exactly the conditions expected in the HFIR, the results indicate that 6061 aluminum has a very high probability of being a satisfactory cladding material for the HFIR fuel plates, provided the pH of the water is maintained at 5.0 or even 5.3 with nitric

acid. Corrosion damage, per se, does not appear to be a problem, and although somewhat excessive temperatures are probable at the hot spots, the great majority of the fuel plates will operate at reasonable temperatures.

ACKNOWLEDGMENT

The authors wish to express their appreciation to M. T. Kegley, who carried out the metallographic examinations of the test specimens and prepared the photographs used in this report.

REFERENCES

1. T. E. Cole, High-Flux Isotope Reactor - A General Description, ORNL CF-60-3-33 (Mar. 15, 1960).
2. J. R. McWherter et al., Preliminary Design of the HFIR Core and Pressure Vessel Assembly, ORNL CF-61-8-75 (Aug. 25, 1961).
3. N. Hilvety, private communication (Sept. 6, 1961).
4. J. C. Griess, H. C. Savage, T. H. Mauney, and J. L. English, Effect of Heat Flux on the Corrosion of Aluminum by Water. Part I. Experimental Equipment and Preliminary Test Results, ORNL-2939 (Apr. 29, 1960).
5. J. C. Griess, H. C. Savage, T. H. Mauney, J. L. English, and J. G. Rainwater, Effect of Heat Flux on the Corrosion of Aluminum by Water. Part II. Influence of Water Temperature, Velocity, and pH on Corrosion-Product Formation, ORNL-3056 (Feb. 10, 1961).
6. J. E. Draley and W. E. Ruther, "Aqueous Corrosion of Aluminum, Part II," Corrosion 12, 480t-490t (1956).
7. J. L. English, L. Rice, and J. C. Griess, The Corrosion of Aluminum Alloys in High-Velocity Water at 170 to 290°C, ORNL-3063 (June 1, 1961).
8. J. E. Draley and W. E. Ruther, "Aqueous Corrosion of Aluminum, Part I," Corrosion 12, 441t-448t (1956).
9. R. J. Lobsinger and J. M. Atwood, "Corrosion of Aluminum in High-Purity Water," Corrosion 13, 582t-584t (1957).

10. G. Ervin, Jr., and E. F. Osborn, "The System Al_2O_3-H_2O," J. Geology 59, 381-394 (1951).

11. W. R. Gambill and R. D. Bundy, HFIR Heat-Transfer Studies of Turbulent Water Flow in Thin Rectangular Channels, ORNL-3079 (June 5, 1961).

12. Letter from J. L. Brandt, ALCOA Technical Information Department, to T. H. Mauney (June 1961).

13. E. N. Sieder and G. E. Tate, "Heat Transfer and Pressure Drop of Liquids in Tubes," Ind. Eng. Chem. 28, 1429-35 (1936).

14. E. R. G. Eckert and R. M. Drake, Jr., Heat and Mass Transfer, p 212-13, McGraw-Hill, New York, 1959.

15. Alcoa Aluminum Handbook, Aluminum Company of America (1956).

16. R. J. Lobsinger, Summary Report on the Corrosion of Aluminum in High-Temperature Dynamic Water Systems, HW-59778 Rev. (Feb. 1, 1961).

17. J. E. Draley, C. R. Breden, W. E. Ruther, and N. R. Grant, "High-Temperature Aqueous Corrosion of Aluminum Alloys," Proceedings of the Second UN International Conference on the Peaceful Uses of Atomic Energy, Geneva 1958, P/714, Vol. 5, p 113-120, United Nations, New York (1958).

18. J. A. Ayres, R. L. Dillon, and R. J. Lobsinger, "The Use of Aluminum as Fuel Cladding in High-Temperature Water-Cooled Reactors," Proceedings of the Second UN International Conference on Peaceful Uses of Atomic Energy, Geneva 1958, P/1430, Vol. 5, p 153-56, United Nations, New York (1958).

19. D. R. DeHalas, A Study of Heat Transfer Effects on Aluminum Corrosion, Part I, HW-42585 Rev. (Apr. 19, 1956).

20. G. J. Biefer and P. G. Anderson, Corrosion Behaviour of Aluminum-Nickel-Iron Alloys in High Temperature Water Under Dynamic Conditions, CRMet-799 (Chalk River, Ontario) (Dec. 1958).

21. C. R. Breden and N. R. Grant, Summary of Corrosion Investigations on High-Temperature Aluminum Alloys, ANL-5546 (Feb. 1960).

APPENDIX

Equations used in calculating the experimental fluid-film heat-transfer coefficients (h) and the thermal conductivity of the corrosion-product layer (k):

Calculation of average heat flux under thick-walled section, Q_a:

$$\Delta t_c = (t_o - t_i)$$

$$H_c = WCp\Delta t$$

$$Q_a = 0.8\ H_c/A$$

Calculation of local heat flux, Q_L:

$$T_a = \frac{\Sigma\ T_L}{n}$$

R_a at T_a from Fig. 15

R_L at T_L from Fig. 15

$$R_r = R_L/R_a$$

$$Q_L = R_r \cdot Q_a$$

Calculation of temperature drop across the specimen metal wall, ΔT_w:

k_L at T_L from Fig. 15

$$\Delta T_w = \frac{Q_L\ x_w}{2\ k_L}$$

Calculation of the coolant temperature at the point, t_L:

$$t_L = t_i + \frac{x}{L}(\Delta T_c)$$

Calculation of fluid-film heat-transfer coefficient, h:

$$\left(T_{ow} \right)_i = T_s - \Delta T_w \text{ (at time zero only)}$$

$$\left(\Delta t_f \right)_i = T_{ow} - t_L \text{ (at time zero only)}$$

$$h_i = Q_L/\Delta t_f$$

Calculation of temperature drop across the oxide,

$$\Delta T_{ox} = T_s - \Delta T_w - \left(\Delta t_f \right)_e - t_L$$

Where

T_s = Temperature as measured on the outside surface of the specimen.

Calculation of the thermal conductivity of the oxide, k_{ox}:

$$k_{ox} = \frac{Q_L \, x_{ox}}{\Delta T_{ox}}$$

Specimen dimensions and areas used in calculations:

Length of specimen	0.5417 ft
Heat-transfer surface area under thick-walled section	0.0271 ft^2
Total heat-transfer surface area	0.0496 ft^2
Thick-walled section cross-sectional area	4.16×10^{-4} ft^2
Total cross-sectional area of specimen	5.02×10^{-4} ft^2
Coolant channel cross-sectional area	1.74×10^{-4} ft^2
Equivalent diameter of coolant channel	7.57×10^{-3} ft
Wall thickness (thick-walled portion)	0.00833 ft

Definition of terms and symbols:

A = Surface area under the thick-walled portion of the specimen (ft^2)

C_p = Heat capacity of water (Btu/lb·°F)

D_e = Equivalent diameter of flow channel (ft)

F = Coolant flow rate (gpm)

h = Fluid-film heat-transfer coefficient (Btu/°F·ft^2·hr)

H_c = Heat removed by the coolant (Btu/hr)

H_e = Electrical heat input

k = Thermal conductivity (Btu·ft/hr·ft^2·°F/ft)

L = Axial length of heated section (ft)

Nu = Nusselt No. $\frac{h \, D_e}{k}$, dimensionless

n = Number of points

Pr = Prandtl number $\left(\frac{C_p \, \mu}{k} \right)$, dimensionless

Q = Heat flux (Btu/ft^2·hr)

R = Electrical resistivity (μohm-cm)

Re = Reynolds No. = $\frac{D_e v \rho}{\mu}$, dimensionless

R_r = Ratio of electrical resistivity at two temperatures

t = Temperature of coolant (°F)

T = Temperature of specimen surface (°F)

v = Fluid velocity (ft/sec)

W = Coolant flow rate (lb/hr)

x = Thickness of heated wall or local axial length to a particular point measured from beginning of heated length (ft)

μ = Viscosity (lb/ft hr)

ρ = Fluid density (lb/ft^3)

ΔT or Δt = Temperature drop (°F)

Subscripts:

a = Average

b = Bulk properties

c = Refers to coolant

e = End of run

f = Fluid film

h = Heated part

i = Inlet or initial

L = Point properties

o = Outlet

ox = Property of the oxide

s = Refers to specimen

w = Refers to the metal wall of the specimen

x = A particular point

ow = Oxide-water interface

ORNL-3230
UC-25 — Metals, Ceramics, and Materials
TID-4500 (16th ed., Rev.)

INTERNAL DISTRIBUTION

1. Biology Library
2-3. Central Research Library
4. Reactor Division Library
5. ORNL — Y-12 Technical Library
Document Reference Section
6-25. Laboratory Records Department
26. Laboratory Records, ORNL R.C.
27. G. M. Adamson
28. A. L. Bacarella
29. J. E. Baker
30. J. M. Baker
31. C. J. Barton
32. C. F. Bayes
33. R. J. Beaver
34. D. S. Billington
35. F. F. Blankenship
36. A. L. Boch
37. E. G. Bohlmann
38. E. S. Bomar
39. G. E. Boyd
40. R. B. Briggs
41. R. D. Bundy
42. D. W. Cardwell
43. T. G. Chapman
44. R. D. Cheverton
45. H. C. Claiborne
46. C. W. Collins
47. E. L. Compere
48. F. L. Culler
49. J. E. Cunningham
50. R. J. Davis
51. J. L. English
52. J. H. Frye, Jr.
53. W. R. Gambill
54-63. J. C. Griess
64. H. Grimac
65. W. R. Grimes
66. D. N. Hess
67. J. W. Hill
68. N. Hilvety
69. L. B. Holland
70. G. H. Jenks
71. D. T. Jones
72. R. G. Jordan (Y-12)
73. P. R. Kasten
74. M. T. Kelley
75. M. J. Kelly
76. J. A. Lane
77. C. E. Larson
78. R. A. Lorenz
79. R. N. Lyon
80. H. G. MacPherson
81. D. W. Magnuson
82. W. D. Manly
83. W. L. Marshall
84. T. H. Mauney
85. H. F. McDuffie
86. H. A. McLain
87. J. R. McWherter
88. J. P. Murray (K-25)
89. P. D. Neumann
90. L. C. Oakes
91. P. Patriarca
92. S. A. Reed
93. L. Rice
94. D. M. Richardson
95. H. C. Savage
96. R. E. Schappel
97. C. H. Secoy
98. A. J. Shor
99. M. J. Skinner
100. I. Spiewak
101. J. A. Swartout
102. A. Taboada
103. J. W. Tackett
104. E. H. Taylor
105. W. C. Thurber
106. G. M. Watson
107. A. M. Weinberg
108. J. C. White
109. E. A. Wick
110. C. E. Winters
111. L. F. Woo
112. F. Daniels (consultant)
113. F. T. Gucker (consultant)
114. F. T. Miles (consultant)

EXTERNAL DISTRIBUTION

115. J. A. Ayres, Hanford Atomic Products Operations
116. D. R. deBoisblanc, Phillips Petroleum Company, Idaho Falls
117. R. L. Dillon, Hanford Atomic Products Operations
118. G. N. Flannagan, Savannah River Operations Office
119. N. Hackerman, Consultant, University of Texas
120. A. A. Johnson, Savannah River Operations Office

121. F. Kreusi, Savannah River Operations Office
122. J. G. Rainwater, University of Arkansas
123. Division of Research and Development, AEC, Washington
124. Division of Research and Development, AEC, ORO
125. Division of Reactor Development, AEC, Washington
126. Division of Reactor Development, AEC, ORO
127-701. Given distribution as shown in TID-4500 (16th ed., Rev.) under Metals, Ceramics, and Materials category (75 copies – OTS)